Journal of Medicinal Chemistry

ARTICLE

pubs.acs.org/jmc

Discovery and Preclinical Evaluation of a Novel Class of Cytotoxic Propynoic Acid Carbamoyl Methyl Amides (PACMAs)

Roppei Yamada,[†] Xuefei Cao,[†] Alexey N. Butkevich,[¶] Melissa Millard,[†] Srinivas Odde,[†] Nick Mordwinkin,[§] Rambabu Gundla,[†] Ebrahim Zandi,[#,‡] Stan G. Louie,[§,‡] Nicos A. Petasis,[¶,‡] and Nouri Neamati*[,†,‡]

[†]Department of Pharmacology and Pharmaceutical Sciences, School of Pharmacy, [¶]Department of Chemistry and Loker Hydrocarbon Research Institute, USC College, [§]Department of Clinical Pharmacy and Pharmaceutical Economics & Policy, School of Pharmacy, [#]Department of Molecular Microbiology and Immunology, Keck School of Medicine, and [‡]Norris Comprehensive Cancer Center, Keck School of Medicine, University of Southern California, Los Angeles, California, 90089

Supporting Information

ABSTRACT: Herein, we discovered a series of propynoic acid carbamoyl methyl-amides (PACMAs) with potent cytotoxicity against a panel of cancer cell lines. These compounds interrupted cell cycle progression at low micromolar concentrations and induced early and late stage apoptosis. A representative compound suppressed tumor growth without apparent toxicity in an MDA-MB-435 mouse xenograft model. We used a Kinexus 628-antibody microarray and the Ingenuity Pathway Analysis (IPA) bioinformatics tools to better understand their mechanisms. The IPA analysis revealed the initiation of Nrf2-mediated oxidative stress through modulating the expression of SOD1 and STIP1 by compound **1**. The involvement of the oxidative stress pathway was further validated by measuring the levels of the PACMA-induced mitochondrial superoxide species. To our knowledge, this is the first report on the discovery and biological evaluations of PACMAs as anticancer agents. Their broad-spectrum *in vitro* cytotoxicity, possibly through an oxidative stress-mediated pathway, and *in vivo* efficacy warrant further preclinical investigations.

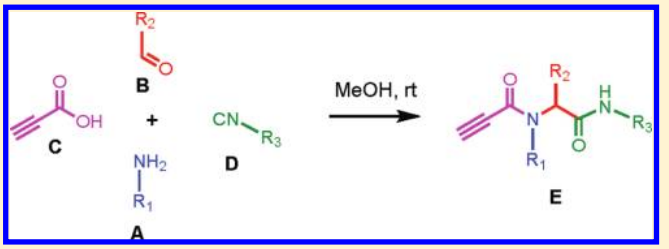

INTRODUCTION

Conventional cytotoxic chemotherapies have proven effective in curing and reducing the risk of recurrence for certain types of cancers. Despite great strides achieved in the design and discovery of novel anticancer agents, there is still a dire need to develop highly effective and safe anticancer medications.[1,2] The early phase drug discovery process usually includes lead identification, lead optimization, target identification/validation, and preclinical evaluations.[3] The initial focus of lead identification through random screening is to select compounds with desired *in vitro* biological activities and drug-like properties from a chemically diverse library of small molecules. Evaluation of pharmacokinetics (PK), pharmacodynamics (PD), and metabolism of the active compounds by calculating selective physicochemical properties important for absorption, distribution, metabolism, excretion, and toxicity (ADMET) is also essential to ensure the drug discovery process to be successful and cost-effective. It is noteworthy that a major hurdle to overcome in random screening is to identify lead compounds with cancer cell-specific toxicity and selective molecular targets. An emerging technology in elucidating the molecular targets and possible mechanisms of action of a pharmacological agent is the application of bioinformatics tools that allow detailed pathway analysis. It is now widely accepted that bioinformatics technology plays a vital role in the interpretation and exploitation of genomic and proteomic data for in-depth understanding of the molecular mechanisms of diseases and drug actions.[4,5]

In an effort to discover novel lead compounds for potential anticancer drugs, we carried out cell-based high-throughput screening (HTS) of our diverse in-house library of 10 000 compounds using 3-(4,5-dimethylthiazol-2-yl)-2,5-diphenyltetrazolium bromide (MTT) assays. Using this method, we identified two cytotoxic propynoic acid carbamoyl methyl amides (PACMAs), compounds **1** and **2**, as potential leads. To develop a preliminary structure−activity relationship (SAR), we further performed a substructure search within our multiconformational small molecule database containing 10 million compounds. Seventeen additional compounds were found to possess chemical structures similar to the original leads. An additional 61 compounds lacking the propynamide moiety were also selected from the similarity search and found to be inactive, implying the essential role of the propynamide group in eliciting cytotoxicity, and not further pursued. Importantly, all active compounds met desirable ADMET criteria and possessed favorable PK characteristics as indicated by our computational simulations, suggesting that human clinical trials may be successful with these compounds.

Received: December 31, 2010
Published: March 28, 2011

In our current study, we evaluated the therapeutic potential of these PACMA compounds in a panel of cancer cell lines and explored the molecular pharmacology of selected active compounds. Our results indicated that compound **4** interrupted cell cycle progression and induced apoptosis in MDA-MB-435 cells. Additionally, we also evaluated the *in vivo* therapeutic potential of compound **2** in an MDA-MB-435 mouse xenograft model. To understand the mechanisms underlying their cytotoxicity, we analyzed compound **1**-treated cell lysates using a Kinexus 628-antibody microarray and the Ingenuity Pathway Analysis (IPA) bioinformatics platform in search of potential signaling transduction networks.

RESULTS AND DISCUSSION

Chemistry. The propynoic acid carbamoyl methyl amide compounds (PACMAs) investigated herein, were conveniently prepared in a single step as shown in Scheme 1 by employing the four-component Ugi reaction.[6−8] Each of the corresponding PACMA compounds **1**−**19** (Scheme 2) were obtained in good yields by reacting equimolar amounts of a primary amine or aniline component **A**, an aryl or heteroaryl aldehyde **B**, propynoic acid **C**, and a cycloalkyl or benzyl isocyanide **D** in methanol at room temperature over 48 h, followed by purification via chromatography and recrystallization.

Drug-like Properties of the PACMA Compounds. Oral bioavailability is a desirable property of investigational compounds in the drug discovery process. Lipinski's rule-of-five is a simplified model to predict the absorption and intestinal permeability of a compound.[9,10] In this model, compounds are considered likely to be well absorbed when they possess cLogP < 5, molecular weight < 500, number of H-bond donors < 5, and number H-bond acceptors < 10. Earlier studies by Palm et al.[11−13] and Kelder et al.[14] recommend that compounds with polar surface area > 140 Å^2 will likely have poor absorption (<10%), whereas compounds with polar surface area < 60 Å^2 are predicted to show complete absorption (>90%). The calculated atom-based LogP (S+ logP) values of the PACMAs range from 2.2 to 4.4, and H-bond donor and acceptor counts are <5 and <10, respectively. As shown in Figure 1 and Table 1, all active (except **4** and **9**) PACMA compounds fall within the desirable range favoring excellent oral bioavailability, whereas the reference compounds doxorubicin and paclitaxel have maximum polar surface areas of >150 Å^2, and camptothecin has a moderate polar surface area of 103 Å^2. In conclusion, all PACMA compounds demonstrate desirable physicochemical properties and, therefore, are potentially promising for further optimization and experimental evaluations.

PACMAs Exhibit Cytotoxicity at Low Micromolar Concentrations in a Panel of Human Cancer Cell Lines. The 19 PACMA compounds were tested in eight human cancer cell lines derived from different tumor origins, including the MDA-MB-435 breast cancer, HCT116 p53$^{+/+}$, HCT116 p53$^{-/-}$, and HT29 colon cancer, HEY and doxorubicin-resistant NCI/ADR-RES ovarian cancer, and UMUC3 and 5637 bladder cancer cell lines (Table 2 and Table S1, Supporting Information). Remarkably, all compounds showed potent cytotoxicity in the NCI/ADR-RES cell line, and in fact, this cell line exhibited the greatest sensitivity to these compounds (Table 2; Figure S1B, Supporting Information). NCI/ADR-RES cells have been shown to overexpress multidrug resistance transporters and *p*-glycoproteins,[15,16] which represents the most common mechanisms for acquisition of resistance by cancer cells.

Scheme 1. General Method for the Synthesis of PACMAs (E)

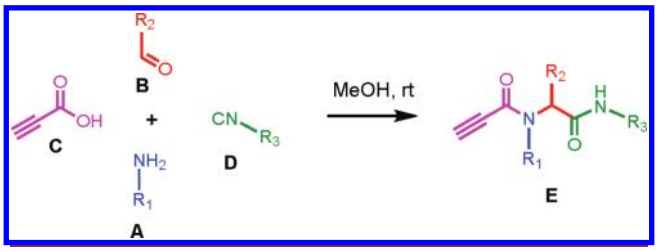

Scheme 2. PACMA Compounds 1−19

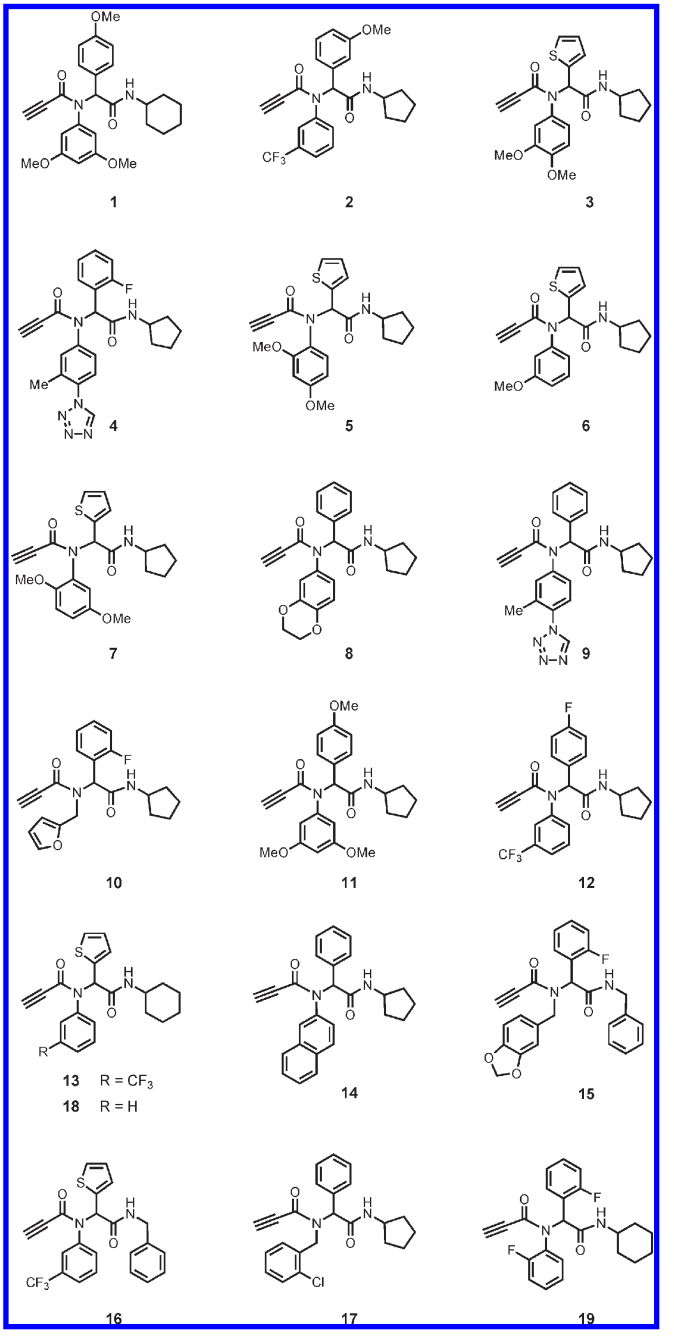

The potent cytotoxicity of these compounds in NCI/ADR-RES cells indicates their promising therapeutic potential for treatment

dx.doi.org/10.1021/jm101655d |*J. Med. Chem.* 2011, 54, 2902–2914

Table 1. Physicochemical Properties of PACMA Compounds Calculated by Computational Simulation[a]

compound	MW	MLogP	S+ logP	PSA	HBD	HBA
1	450.5	2.54	3.62	55.18	1	7
2	444.5	3.70	4.20	40.65	1	5
3	412.5	2.26	2.83	49.91	1	6
4	446.5	3.91	2.81	122.06	1	7
5	412.5	2.26	2.86	44.69	1	6
6	382.5	2.55	2.99	49.85	1	5
7	412.5	2.26	2.74	45.72	1	6
8	404.5	2.62	2.97	51.90	1	6
9	428.5	3.54	2.63	129.21	1	7
10	368.4	2.39	2.27	43.08	1	5
11	436.5	2.33	3.23	54.79	1	7
12	432.4	4.38	4.67	32.99	1	4
13	434.5	3.88	4.53	39.73	1	4
14	410.5	4.11	4.93	37.34	1	4
15	444.5	3.32	3.41	57.05	1	6
16	442.5	3.86	4.26	42.75	1	4
17	429.3	4.11	4.11	27.71	1	4
18	366.5	3.07	3.35	31.53	1	4
19	396.5	4.17	4.24	31.57	1	4
camptothecin	348.4	1.67	1.60	103.63	1	5
doxorubicin	543.5	−0.82	0.54	233.93	6	12
paclitaxel	839.9	0.54	3.66	156.48	4	15

[a] MW, molecular weight; MLogP, Moriguchi octanol−water partition coefficient; S+ logP, SimulationsPlus, Inc., model of logP; PSA, three-dimensional polar surface area; HBD, hydrogen-bond donor; HBA, hydrogen-bond acceptor.

of human cancers that have developed resistance to standard chemotherapeutic agents, such as doxorubicin and paclitaxel. In addition to NCI/ADR-RES cells, Rb-null 5637 cells were also sensitive to these compounds, whereas Rb-expressing UMUC3 cells were the least sensitive among the cell lines tested (Table 2). When tested in MDA-MB-435 cells, compound **9** appeared to be the most potent analogue (Figure 2A). Among the selected cell lines, **4** showed remarkable potency in 5637 cells (Figure 2B). It has been reported that 5637 bladder cancer cells lack a functional Rb protein and are highly metastatic.[17,18] On the basis of observed Rb-dependency by these compounds, they are predicted to have potential applications in highly malignant bladder cancers.[19,20] To further confirm the MTT

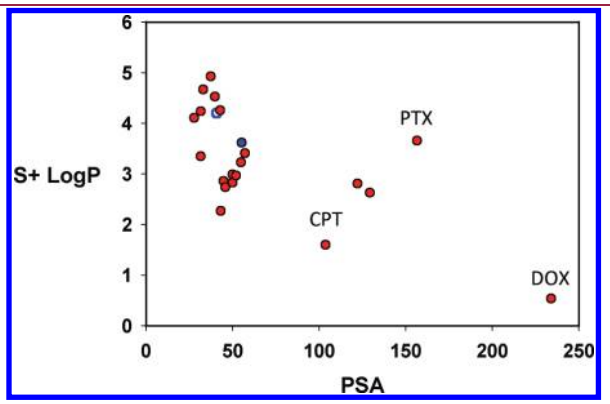

Figure 1. Prediction of drug absorption by computational simulation. 3-D Polar surface area in Å^2 versus partition coefficient (S+ logP) calculated by ADMET Predictor.

Table 2. *In Vitro* Cytotoxicity of Compounds 1−19 in a Panel of Human Cancer Cell Lines

	IC_{50}[a] (μM)							
compound	HT29	HCT116 p53$^{+/+}$	HCT116 p53$^{-/-}$	HEY	MDA-MB-435	UMUC3	5637	NCI/ADR-RES
1	6.3 ± 1.5	12.5 ± 2.1	11.0	4.4 ± 3.0	5.4 ± 2.9	>20	2.2 ± 0.2	0.3 ± 0.0
2	7.2 ± 0.2	>10	8.8 ± 0.4	5.2 ± 3.4	6.3 ± 1.1	>20	0.6 ± 0.4	0.2 ± 0.1
3	5.5 ± 4.2	7.7 ± 1.9	9.6 ± 4.9	3.4 ± 1.5	2.0 ± 0.1	>20	2.0 ± 0.7	0.9 ± 0.8
4	1.8 ± 1.7	6.3 ± 1.8	5.5 ± 0.7	1.5 ± 0.8	1.4 ± 0.2	6.3 ± 1.0	0.7 ± 0.5	1.0 ± 0.3
5	2.3 ± 0.3	6.9 ± 0.6	7.0 ± 0.7	4.1 ± 3.4	1.7 ± 0.5	>20	1.7 ± 0.8	0.4 ± 0.0
6	2.3 ± 0.3	7.2 ± 0.2	5.6 ± 0.8	1.9 ± 0.7	1.7 ± 0.4	6.9 ± 1.2	0.3 ± 0.0	0.3 ± 0.0
7	1.6 ± 1.0	5.7 ± 0.6	4.7 ± 2.3	1.5 ± 1.1	0.5 ± 0.3	5.7 ± 1.5	0.3 ± 0.0	0.3 ± 0.0
8	3.2 ± 1.2	17.3 ± 1.1	>20	4.1 ± 3.4	1.8 ± 0.6	>20	1.9 ± 0.6	0.3 ± 0.0
9	1.5 ± 1.1	7.2 ± 0.2	5.7 ± 0.9	1.9 ± 0.3	0.6 ± 0.3	7.8 ± 1.8	0.4 ± 0.1	1.0 ± 0.7
10	>10	10.5	13.0 ± 2.8	4.3 ± 3.9	1.7 ± 0.6	>20	2.9 ± 0.8	1.2 ± 0.4
11	2.1 ± 0.4	15.0	>20	2.3 ± 0.4	2.4 ± 0.1	>20	1.9 ± 0.6	0.3 ± 0.0
12	4.8 ± 3.2	7.5 ± 0.7	6.9 ± 0.6	2.4 ± 0.2	5.2 ± 1.2	8.0 ± 1.4	0.5 ± 0.3	0.4 ± 0.0
13	6.0 ± 1.4	8.3 ± 1.1	10.4 ± 0.2	5.2 ± 3.6	6.9 ± 0.8	>20	1.6 ± 0.7	0.4 ± 0.0
14	4.9 ± 3.4	6.8 ± 1.8	7.4 ± 0.8	1.7 ± 1.1	7.3 ± 0.0	>20	0.5 ± 0.3	0.3 ± 0.0
15	>10	>10	>20	>10	>10	>20	2.8 ± 1.1	1.3 ± 1.0
16	7.3 ± 0.3	9.0 ± 1.4	16.1 ± 5.6	7.1 ± 2.6	4.2 ± 3.0	>20	1.2 ± 1.1	0.7 ± 0.6
17	5.4 ± 3.0	7.7 ± 0.5	7.3 ± 1.4	5.8 ± 1.3	8.2 ± 0.2	>20	1.8 ± 0.1	2.2 ± 0.2
18	>10	14.0	>20	>10	>10	>20	3.5 ± 1.4	1.3 ± 0.4
19	7.7 ± 0.5	11.9 ± 0.1	10.1 ± 2.9	5.6 ± 2.1	6.5 ± 2.1	>20	2.1 ± 0.0	0.4 ± 0.1

[a] Cytotoxic concentration (IC_{50}) is defined as drug concentration causing a 50% decrease in cell population using MTT assay as described in the Experimental Section.

dx.doi.org/10.1021/jm101655d |*J. Med. Chem.* 2011, 54, 2902–2914

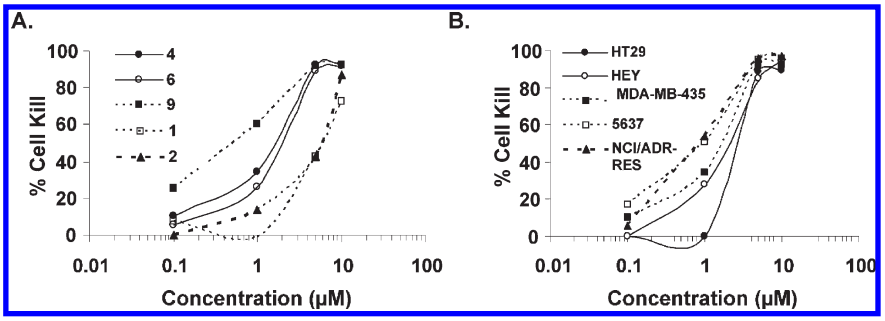

Figure 2. Cytotoxicity of selected PACMA compounds in a panel of cancer cell lines. (A) The IC_{50} values of **1**, **2**, **4**, **6**, and **9** in MDA-MB-435 cells range from 0.6 to 6.3 μM. (B) The IC_{50} values of compound **4** range between 1 and 2.5 μM in tested cell lines using MTT assays.

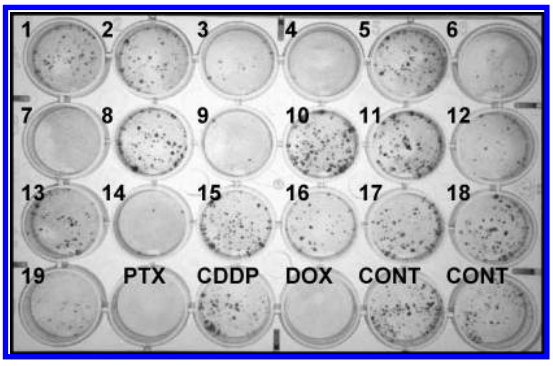

Figure 3. Colony formation assay of the active PACMA compounds in MDA-MB-435 cells. MDA-MB-435 cells were treated with 1 μM PACMA compounds. The colony formation observations were consistent with the MTT results. Abbreviations are as follows: PTX, paclitaxel; CDDP, cisplatinum; CONT, vehicle (DMSO) control.

observations, we performed colony formation assays on all compounds at 1 μM in MDA-MB-435 cells (Figure 3). The results were conclusive and consistent with the MTT observations. In addition to these 19 compounds, we also tested 61 compounds without the propynamide functional group in MDA-MB-435 cells, and 13 compounds exhibited moderate cytotoxicity around 40% at 10 μM (data not shown). However, when tested in NCI/ADR-RES cells, they failed to inhibit colony formation (Figure S1A, Supporting Information), suggesting the critical function of the propynamide moiety in inducing cytotoxicity of this class of compounds.

Compound 2 Exhibits Promising *in Vivo* Efficacy in an MDA-MB-435 Mouse Xenograft Model. To investigate the *in vivo* efficacy of these compounds, we selected compound **2** and evaluated its anticancer activity in a nude mouse xenograft model using MDA-MB-435 cells. Animals were treated with daily intraperitoneal (i.p.) injections of DMSO in sesame oil (vehicle control) or compound **2** at 10 mg/kg for 9 days, followed by 20 mg/kg for 5 days and concluding with 40 mg/kg for 12 days. After 26 days of dosing, the drug treatment was discontinued. Mice were monitored daily for an additional 17 days, and tumors were measured twice per week. Figure 4A summarizes the tumor volume (mean ± SEM) of the treatment groups throughout the observation time. Compound **2** significantly reduced tumor burden in this xenograft model. The possible toxicity elicited by **2** was also evaluated by following the body weight of the mice over the course of treatment and histological examination of the organs. The treatment was well-tolerated and did not result in any drug-related death or body weight loss (Figure 4B). Specifically, the untreated control mice had an average weight of 23 ± 2 g (mean ± SD) before the experiment and 28 ± 2 g after the experiment. Mice treated with **2** had a comparable average weight of 29 ± 2 g after treatment. Furthermore, histopathological examinations of the organs derived from at least three mice in the treatment group showed no histological evidence of organ toxicity (data not shown).

Compound 4 Induces S and G_2/M Cell Cycle Arrest in MDA-MB-435 Cells. Compound **4** is one of the most active compounds in the MDA-MB-435 cell line (Table 2). Hence, we selected this compound for further examination to determine its ability to induce cell cycle perturbation in MDA-MB-435 cells. Cells were treated with **4** for 6, 12, and 24 h. The analysis of DNA profiles by flow cytometry demonstrated that **4** was able to block cell cycle progression at both S and G_2/M phases (Figure 5). In particular, at 24 h, there was a 10% and 7% increase in the number of cells retained in S and G_2/M phases, respectively, when compared with untreated control cells. The property of compound **4** to disrupt cell cycle progression makes it an interesting agent for combination treatments with drugs acting at different stages of cell cycle.

Compounds 1, 2, and 4 Trigger Apoptosis. Most cytotoxic anticancer drugs induce apoptosis.[21] To understand the mechanisms underlying the cytotoxicity of PACMAs, we measured the percentage of early and late apoptotic cells in MDA-MB-435 cells treated with compounds **1**, **2**, and **4**, respectively, by flow cytometry. An early event in apoptotic cell death is the translocation of phosphatidyl-serine residues to the outer cell membrane. This event precedes nuclear breakdown, DNA fragmentation, and appearance of most apoptosis-associated molecules and is readily distinguished from the late apoptotic processes by annexin V/propidium iodide binding assay. As shown in Figure 6, the percentage of early apoptotic cells reached 24% after 48 h exposure to compound **4** and the ratio of late apoptotic cells was significantly increased to 27% and 62% after 24 and 48 h treatment, respectively. The original lead compounds, **1** and **2**, failed to induce early apoptosis at 24 h, and the early apoptotic cells were slightly increased by 8% after 48 h treatment. However, the percentage of late apoptotic cells reached 35% and 37% for **1** and **2**, respectively, after 48 h treatment, suggesting a less marked and delayed induction of apoptosis by these two compounds. Taken together, these observations implied that apoptosis might be one of the mechanisms utilized by these compounds to elicit cytotoxicity. It is known that apoptosis signaling pathways have a profound effect on both cancer progression and response to chemotherapy.[22−24]

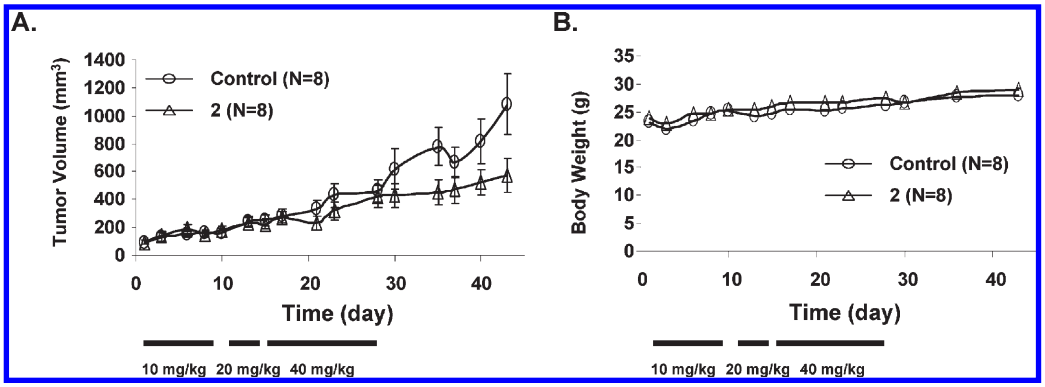

Figure 4. Compound **2** showed *in vivo* efficacy in an MDA-MB-435 mouse xenograft model. (A) Compound **2** reduced tumor burden. Athymic nude mice implanted with MDA-MB-435 cells were treated with indicated doses of **2** by i.p. administration 5 times weekly. Values represent the tumor volumes (mean ± SEM) for each group. (B) Compound **2** treatment did not cause weight loss. This compound was well-tolerated and did not result in any drug-related deaths or changes in body weight.

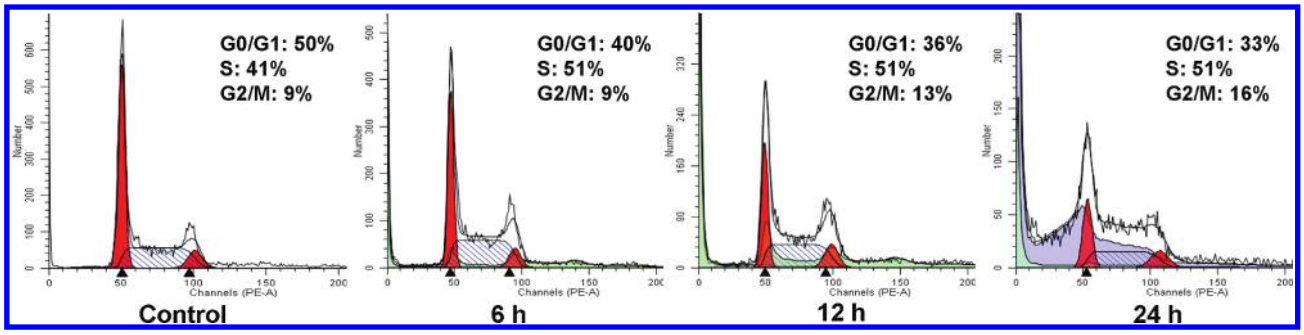

Figure 5. Cell cycle profiles of MDA-MB-435 cells treated with compound **4**. Cells were treated with 5 μM compound **4** for 6, 12, and 24 h, collected, stained with propidium iodide, and analyzed for perturbation of cell cycle by flow cytometry. Compound **4** induced both S and G_2/M arrest.

A great number of genes are involved in apoptosis and have been found to be defective in a high percentage of human malignancies.[25] Thus, reactivation of apoptosis pathways by modulating apoptosis-related proteins is an attractive and growing trend for anticancer drug discovery. Currently, we are in the process of identifying the apoptosis-related proteins involved and elucidating the specific apoptotic signaling pathways initiated by these compounds.

Compound 1 Targets Pro-apoptotic p53 and Caspase-9. Among the proteins associated with apoptosis signaling, p53 and caspase-9 are the most commonly activated pro-apoptotic proteins by apoptosis-inducing agents. Thus, as a preliminary mechanistic investigation, we examined the cellular effect of the original lead compound **1** on apoptotic signaling through the protein expression changes of p53 and caspase-9. As shown in Figure 7A, the protein level of p53 was up-regulated by **1** after 24 h treatment and the activation of p53 was sustained for 72 h (lanes 4−6 versus lane 1), suggesting the involvement of p53 in compound **1**-mediated cytotoxicity. Several lines of evidence have demonstrated the activation of caspases during p53-mediated apoptosis in both cell-based and cell-free systems.[26,27] We, therefore, measured the protein levels of full-length caspase-9 in response to compound **1** treatment by Western blotting. A 2-fold decrease in the full-length caspase-9 protein level was observed after 24 h, and the change was maintained up to 72 h (Figure 7B). These observations led us to hypothesize that the decrease in full-length caspase-9 protein level is due to its cleavage and activation in response to apoptotic signaling initiated by compound **1**. This suggests that compound **1** elicits cytotoxicity through activating p53 as well as the downstream signaling cascades of p53-mediated apoptotic events.

Signaling Network Analysis Using the Ingenuity Pathway Analysis (IPA) Platform. To better understand the mechanisms of action of this class of novel PACMA compounds, we subjected cell lysates from untreated and compound **1**-treated MDA-MB-435 cells to the Kinexus 628-antibody microarray analysis in search of potential signaling molecules; 350 pan-specific and 270 phospho-site antibodies were included to track changes in protein expression and phosphorylation status. The cell lysates were run in parallel on the Kinexus antibody chip and the differential binding of dye-labeled proteins was detected and quantified. Proteins with significant expression changes were then identified and used as the basis for signaling pathway interpretation.

To visualize and understand the signaling networks affected by compound **1**, we uploaded the sets of significantly altered pan-specific proteins to the IPA bioinformatics platform. All proteins uploaded were recognized by the IPA software as being eligible for pathway analysis. Several pathways were proposed as a result of the knowledge-based data curation (Figure 8A). The major putative canonical pathway suggested by the IPA was the oxidative stress signaling pathway mediated by Nrf2 (nuclear factor erythroid 2-related factor 2).[28−30] This pathway had a *p*-value of 5.82×10^{-5}, based on the expression changes of several kinases and transcription factors identified in the Nrf2-mediated oxidative stress pathway, including protein kinase C (PKC),

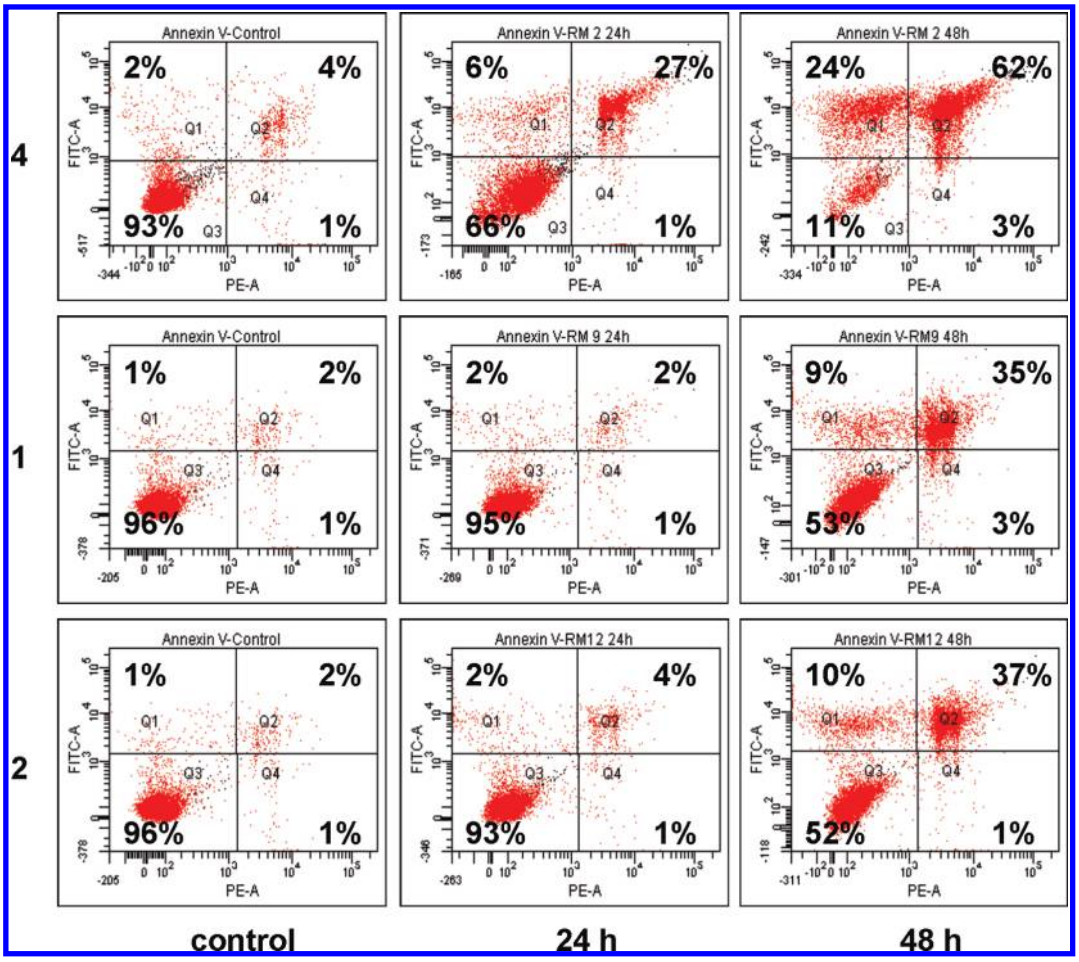

Figure 6. Compounds **1**, **2**, and **4** induce apoptosis. Cells were treated with compounds **1**, **2**, and **4** for 24 and 48 h, stained with annexin V/propidium iodide, and analyzed by flow cytometry. Untreated control cells (48 h) were also included in the analysis. Cells in the bottom left quadrant (annexin V-negative, propidium iodide-negative) are viable, whereas cells in the top left quadrant (annexin V-positive, propidium iodide-negative) are in the early stages of apoptosis, and the cells in the top right quadrant (annexin V-positive, propidium iodide-positive) are in later stages of apoptosis and necrosis.

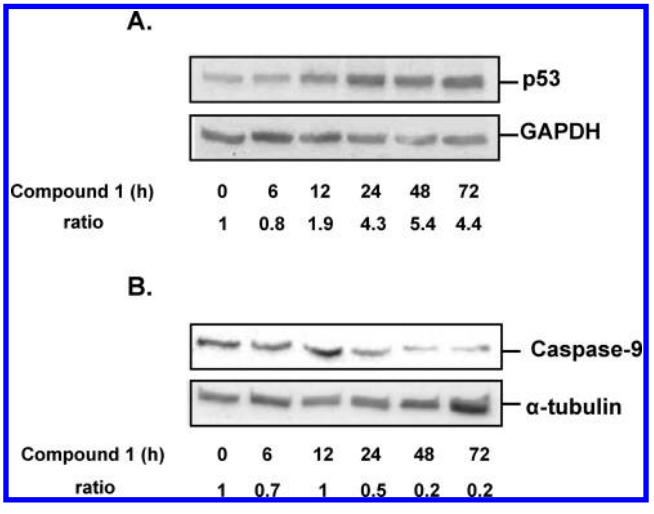

Figure 7. p53 and caspase-9 protein expression in MDA-MB-435 cells treated with 1 μM compound **1**. (A) p53 was up-regulated by **1** in a time-dependent manner. (B) The full-length caspase-9 was decreased in response to **1** treatment. Ratios of p53 to GAPDH and full-length caspase-9 to GAPDH were determined using the ImageQuant (GE Healthcare).

STIP1, MAPK3, and superoxide dismutase 1 (SOD1) (Figure 8B). Reactive oxygen species (ROS), such as superoxide and hydrogen peroxide, are metabolites transiently formed during normal cellular metabolism. However, elevated production of ROS damages most cellular components, and the perturbation of cellular homeostasis, in turn, results in the propagation of more ROS. The positive-feedback loop between ROS production and homeostasis disturbance ultimately causes cell death. Nrf2 is widely expressed in a number of organs and functions as a key sensor for cellular response to oxidative stress, by means of its regulatory function on the transcription of a number of genes encoding antioxidant proteins and related enzymes.[31−34] SOD1 is one of two antioxidant isozymes responsible for scavenging cellular superoxide radicals and was found to be up-regulated by compound **1** in our antibody microarray assay. SOD1 is a downstream target of Nrf2, and it has been reported that Nrf2 activates the transcription of SOD1,[28] which then phosphorylates STAT1 to execute antioxidant responses.[35] In addition to SOD1, Nrf2 may also respond to oxidative stress by activating the mRNA transcription of STIP1.[36] STIP1 functions as a molecular chaperone for heat shock protein 70 (HSP70) and heat shock protein 90 (HSP90). Under nonstress conditions, HSP90, acting as a molecular chaperone, facilitates protein folding and protein

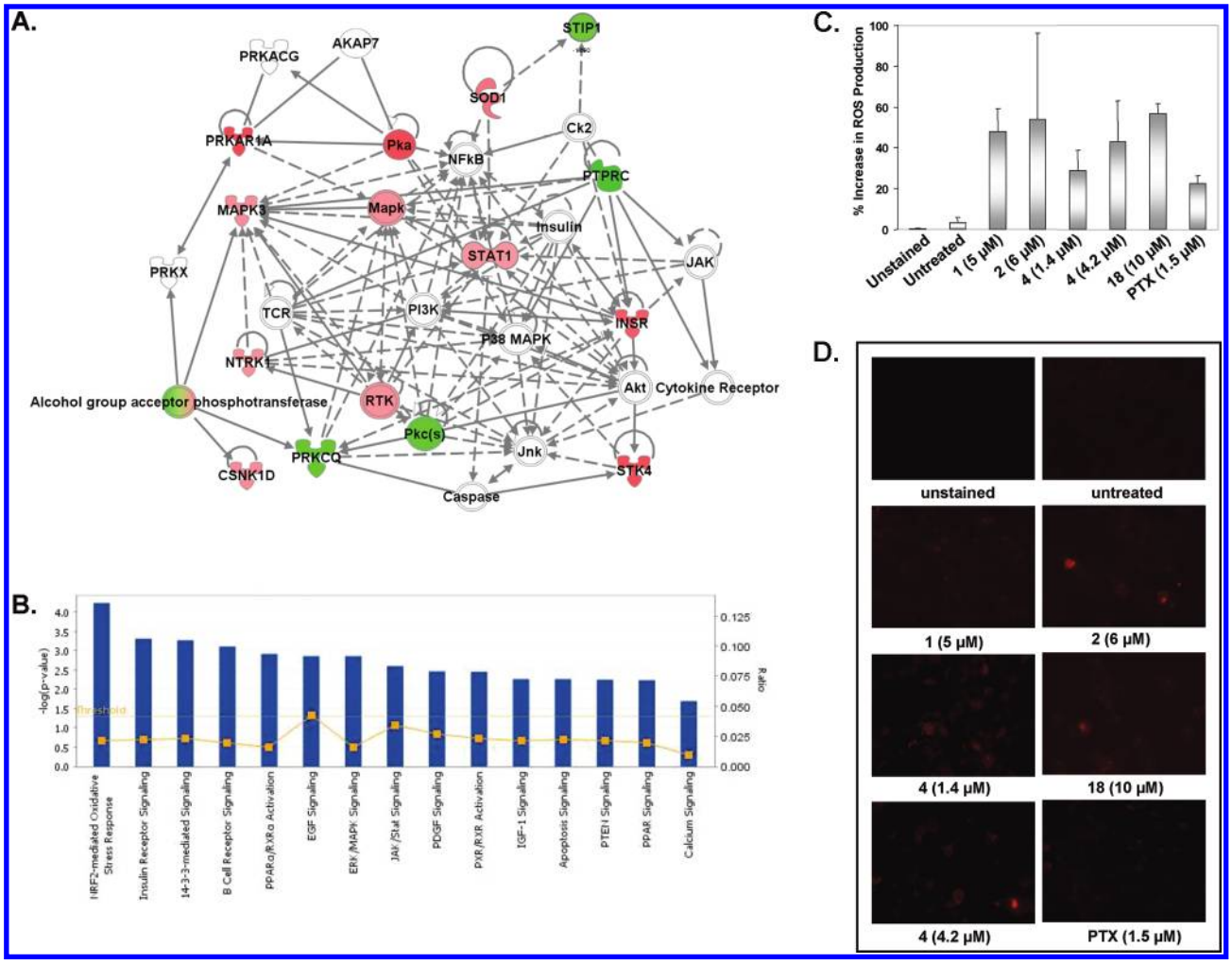

Figure 8. Prediction of compound **1**-mediated signaling pathways using IPA bioinformatics tool. (A) Ingenuity pathway networks of compound **1**-induced cell signaling (score 41) obtained on a set of altered pan-specific proteins. Proteins with their ratio changes and corresponding Swiss-Prot accession numbers were uploaded to IPA software. (—) Direct interaction; (– – –) Indirect interaction. Blue bars represent the −log(*p*-value) of each representative pathway, with the threshold for statistical significance denoted by the thin gray line. Points connected by the solid line represent the ratio of affected molecules versus the total number of molecules in a given pathway. (B) Canonical pathway analysis. Fifteen canonical pathways of interest were selected and presented. (C) Quantification of mitochondrial superoxide production upon drug treatment in MDA-MB-435 cells. Cells were treated with compounds **1**, **2**, **4**, and **18** for 24 h. The untreated and treated cells were incubated with 5 μM MitoSOX for 10 min at 37 °C, collected in Hank's balanced salt solution (HBSS), and subjected to flow cytometric analysis. (D) Examination of mitochondrial superoxide production in response to **1**, **2**, **9**, and **18** treatment in MDA-MB-435 cells. Cells were treated with indicated compounds for 24 h. Untreated and treated cells were incubated with 5 μM of MitoSOX for 10 min at 37 °C and observed under a fluorescence microscope.

degradation to maintain cellular homeostasis. In addition to these functions, HSP90 was recently found to confer antiapoptotic functions by regulating several apoptosis-related molecules.[37,38] Therefore, it is conceivable that down-regulating HSP90 protein expression could abolish HSP90-mediated cell survival. ROS were reported to be able to mediate HSP90 protein cleavage, and this ROS-dependent HSP90 cleavage was involved in arsenic- and MMA-induced apoptosis.[39] On the basis of these reports, it is plausible that compound **1**-induced down-regulation of STIP1 may decrease the amount of HSP90 and, hence, induce apoptosis. Taken together, we hypothesize that compound **1** elicits cytotoxicity by inducing ROS production and further alters the expression of oxidative stress-related proteins, such as SOD1, STIP1, and HSP90. The oxidative stress sensor, Nrf2, may be one of the early proteins activated in response to compound **1** treatment.

Compounds 1, 2, 4, and 18 Induce the Accumulation of Mitochondrial Superoxide. As a preliminary validation of the pathway proposed by IPA, we examined mitochondrial superoxide production by compounds **1**, **2**, **4**, and **18** in MDA-MB-435 cells. Mitochondrial superoxide species was detected using MitoSOX Red mitochondrial superoxide live cell indicator. Cells were treated with these compounds at their respective IC_{50} or $3 \times IC_{50}$ concentrations for 24 h. All compounds were found to induce significant amounts of superoxide upon 24 h treatment (Figure 8C). The flow cytometry observation was further confirmed by examining the staining pattern of mitochondrial superoxide in response to compound treatment by fluorescence microscopy. Consistently, all compounds, including the less active compound **18**, remarkably enhanced the intensity of MitoSOX staining (Figure 8D). Interestingly, paclitaxel only induced a minor amount of mitochondrial superoxide even at

dx.doi.org/10.1021/jm101655d |*J. Med. Chem.* 2011, 54, 2902–2914

Table 3. PK Parameters of Compounds 4 and 9 after i.p. Administration

PK parameters	compound 4	compound 9
C_{max} (ng/mL)	344	6.2
T_{max} (h)	1.0	5
K_{el} (h^{-1})	0.206	0.0
$t_{1/2}$ (h)	3.5	9.3
AUC (ng·h/mL)	520	124.9

1.5 μM (Figure 8D). In addition to mitochondrial superoxide, we also measured the production of other types of reactive oxygen species using 2,7-dichlorodihydrofluorescein (DCFH) staining, and no change was observed (data not shown). Based on these observations, we propose that superoxide induction by PACMAs is a unique mechanism by which these compounds elicit cytotoxicity.

Compounds 4 and 9 Show Favorable Pharmacokinetic Profiles. To assess the efficacy, tolerability, and pharmacokinetics of these novel compounds following i.p. administration, the pharmacokinetic profile of compounds **4** and **9** was evaluated (Table 3). Mice were treated with **4** and **9** via i.p. injection and serial blood sampling was determined at indicated times after administration. The plasma concentration was determined using a validated liquid chromatography−mass spectrometry (LC-MS) method where the lowest level of quantification was 1 ng/mL. One hour following i.p. administration of **4** and **9**, their concentrations in the blood were 344 and 6.2 ng/mL, respectively. Sequential plasma analysis revealed an apparent two compartmental pharmacokinetic elimination (Figure 9). The half-lives of compounds **4** and **9** via i.p. administration were determined to be approximately 3.5 and 9.3 h, respectively, when a noncompartmental pharmacokinetics analysis was used. The favorable pharmacokinetics profile of **4** and **9** is consistent with the ADMET predictions described previously.

In conclusion, the reported propynoic acid carbamoyl methyl amides (PACMAs) are promising anticancer agents with a number of desirable features and presumably operate through an oxidative stress-mediated pathway. Identification of their direct cellular target is beyond the scope of this paper. Of special note is their ability to show significant cytotoxicity in various drug-resistant cell lines. Their broad-spectrum *in vitro* cytotoxicity and *in vivo* efficacy warrant further mechanistic and preclinical investigations. The synthesis of these compounds is quite simple, amenable to parallel as well as large-scale synthesis. We have synthesized numerous other analogs to better understand their pharmacological properties and to carry out in-depth toxicological studies. Results of these latter studies will be reported elsewhere.

EXPERIMENTAL SECTION

Chemistry. All commercially available compounds were used without further purification. 3-Methyl-4-(1*H*-tetrazol-1-yl)aniline was synthesized from commercially available 2-methyl-4-nitroaniline according to the reported procedure.[40] Flash chromatography was performed using Sorbent Technologies 60 Å silica gel (40−63 μm). All final compounds were purified to >95% purity as determined by Varian HPLC instrument with UV detection at 254 nm. Proton (^{1}H), fluorine (^{19}F), and carbon (^{13}C) nuclear magnetic resonance (NMR) spectra were recorded on a Varian Mercury 400 MHz NMR spectrometer. $CDCl_3$ (99.8% D, Cambridge Isotope Laboratories) and DMSO-d_6 (99.9% D, Cambridge Isotope Laboratories) were used in all experiments as indicated. Chemical shifts are reported as parts per million (δ) relative to tetramethylsilane. CF multiplets in ^{13}C NMR spectra are interpreted wherever possible.

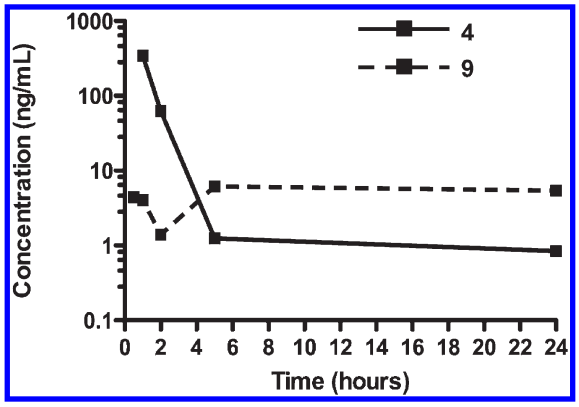

Figure 9. The pharmacokinetics distribution of compounds **4** and **9** in mice. Mice were administered 24 mg/kg of **4** and **9** via i.p. administration. Blood samples were collected at 1, 2, 5, and 24 h for **4** and 0.5, 1, 2, 5, and 24 h for **9**. Plasma concentrations of **4** and **9** are plotted against time. The plasma concentration was determined using a validated LC-MS method where the lowest level of sensitivity is 1 ng/mL.

General Method for the Synthesis of PACMA Compounds (1−19). A solution of the required aniline or benzylamine **A** (2 mmol), aryl or heteroaryl aldehyde **B** (2 mmol), propynoic acid **C** (2.2 mmol), and isocyanide **D** (2.2 mmol) in methanol (2 mL) was stirred at room temperature for 48 h. The products that precipitated from the reaction mixture were filtered off, washed with aqueous methanol (1:1), and recrystallized from ethyl acetate−hexane. Alternatively, the reaction mixture was evaporated to dryness and subject to column chromatography in ethyl acetate−hexane. The fractions containing the target compound were evaporated to dryness, and the product **E** was recrystallized from ethyl acetate−hexane.

*N-[2-(Cyclohexylamino)-1-(4-methoxyphenyl)-2-oxoethyl]-N-(3,5-dimethoxyphenyl) Propynamide (**1**).* Yield 241 mg (54%). ^{1}H NMR (400 MHz, $CDCl_3$): δ 7.07−7.13 (m, 2H), 6.71−6.77 (m, 2H), 6.30−6.45 (m, 3H), 5.86 (s, 1H), 5.53 (br.d, J = 8.3 Hz, 1H), 3.76 (s, 3H), 3.74−3.85 (m, 1H), 3.66 (s, 6H), 2.83 (s, 1H), 1.80−1.96 (m, 2H), 1.51−1.75 (m, 3H), 1.23−1.40 (m, 2H), 0.96−1.17 (m, 3H). ^{13}C NMR (100 MHz, $CDCl_3$): δ 167.7, 160.3, 159.8, 153.5, 140.8, 131.6, 125.8, 113.9, 108.7, 101.3, 80.1, 76.1, 64.8, 55.5, 55.3, 48.8, 32.8, 25.5, 24.8, 24.7.

*N-[2-(Cyclopentylamino)-1-(3-methoxyphenyl)-2-oxoethyl]-N-[3-(trifluoromethyl) phenyl] Propynamide (**2**).* Yield 828 mg (93%). ^{1}H NMR (400 MHz, $CDCl_3$): δ 7.24−7.60 (m, 4H), 7.09 (t, J = 7.9 Hz, 1H), 6.74 (d, J = 7.9 Hz, 1H), 6.68 (d, J = 7.5 Hz, 1H), 6.58 (s, 1H), 6.06 (s, 1H), 5.88 (br.d, J = 7.1 Hz, 1H), 4.20 (sextet, J = 6.6 Hz, 1H), 3.60 (s, 3H), 2.82 (s, 1H), 1.83−2.02 (m, 2H), 1.47−1.65 (m, 4H), 1.33−1.45 (m, 1H), 1.19−1.31 (m, 1H). ^{13}C NMR (100 MHz, $CDCl_3$): δ 167.9, 159.5, 153.3, 139.2, 134.7, 134.5, 130.6 (quartet, J = 33.1 Hz), 129.3, 128.9, 128.0 (quartet, J = 3.7 Hz), 125.1 (quartet, J = 3.7 Hz), 123.3 (quartet, J = 273.6 Hz), 122.5, 115.2, 114.9, 81.1, 75.6, 64.1, 55.1, 51.7, 32.7, 32.6, 23.59, 23.57. ^{19}F NMR (376 MHz, $CDCl_3$): δ −62.72.

*N-[2-(Cyclopentylamino)-2-oxo-1-thien-2-ylethyl]-N-(3,4-dimethoxyphenyl) Propynamide (**3**).* Yield 706 mg (86%). ^{1}H NMR (400 MHz, $CDCl_3$): δ 7.19 (dd, J = 4.9 Hz, J = 1.2 Hz, 1H), 6.91 (br.d, J = 3.3 Hz, 1H), 7.19 (dd, J = 4.9 Hz, J = 3.7 Hz, 1H), 6.60−6.75 (m, 3H), 6.23 (br. d, J = 7.5 Hz, 1H), 6.20 (s, 1H), 4.15 (sextet, J = 6.6 Hz, 1H), 3.77 (s, 3H), 3.65 (s, 3H), 2.84 (s, 1H), 1.82−1.98 (m, 2H), 1.45−1.63 (m, 4H), 1.28−1.43 (m, 2H). ^{13}C NMR (100 MHz, $CDCl_3$): δ 167.1, 153.5,

148.9, 148.2, 135.0, 131.1, 129.7, 127.8, 126.2, 122.7, 113.0, 109.9, 80.6, 75.8, 59.2, 55.7, 55.5, 51.5, 32.6, 32.5, 23.50, 23.46.

*N-[2-(Cyclopentylamino)-1-(2-fluorophenyl)-2-oxoethyl]-N-[3-methyl-4-(1H-tetraazol-1-yl)phenyl] Propynamide (**4**).* Yield 532 mg (60%). ^{1}H NMR (400 MHz, $CDCl_3$): δ 8.81 (s, 1H), 7.23−7.60 (m, 3H), 7.10−7.21 (m, 2H), 6.94−7.08 (m, 2H), 6.38 (s, 1H), 6.22 (br.d, J = 7.1 Hz, 1H), 4.26 (sextet, J = 6.6 Hz, 1H), 2.93 (s, 1H), 2.12 (s, 3H), 1.90−2.07 (m, 2H), 1.43−1.74 (m, 5H), 1.31−1.42 (m, 1H). ^{13}C NMR (100 MHz, $CDCl_3$): 167.4, 160.7 (d, J = 248.5 Hz), 153.0, 142.9, 140.5, 133.9 (d, J = 14.2 Hz), 132.5, 131.2 (d, J = 9.0 Hz), 131.1, 129.5, 125.6, 124.4 (d, J = 2.6 Hz), 120.7 (d, J = 12.9 Hz), 115.4 (d, J = 21.9 Hz), 81.2, 75.6, 70.1, 57.5, 51.8, 32.72, 32.65, 23.6, 17.7. ^{19}F NMR (376 MHz, $CDCl_3$): δ −115.35.

*N-[2-(Cyclopentylamino)-2-oxo-1-thien-2-ylethyl]-N-(2,4-dimethoxyphenyl) Propynamide (**5**).* Yield 453 mg (55%). In $CDCl_3$, mixture of two rotameric forms in 60:40 ratio. ^{1}H NMR (400 MHz, $CDCl_3$): δ 7.34 (d, J = 8.7 Hz, 0.6H), 7.12−7.22 (m, 0.6H+0.4H+0.4H), 7.01 (d, J = 3.3 Hz, 0.4H), 6.91 (d, J = 3.3 Hz, 0.6H), 6.86 (dd, J = 5.4 Hz, J = 3.7 Hz, 0.4H), 6.82 (dd, J = 5.4 Hz, J = 3.7 Hz, 0.6H), 6.53 (d, J = 8.7 Hz, 0.4H), 6.37−6.46 (m, 0.6H+0.6H+0.4H), 6.27 (d, J = 2.5 Hz, 0.6H), 6.22 (dd, J = 8.7 Hz, J = 2.5 Hz, 0.4H), 6.12 (s, 0.4H), 5.99 (s, 0.6H), 4.15−4.27 (m, 0.6H+0.4H), 3.82 (s, 1.2H), 3.78 (s, 1.8H), 3.75 (s, 1.2H), 3.55 (s, 1.8H), 2.74 (s, 0.4H), 2.72 (s, 0.6H), 1.89−2.06 (m, 2 × 0.6H+2 × 0.4H), 1.31−1.75 (m, 6 × 0.6H+6 × 0.4H). ^{13}C NMR (100 MHz, $CDCl_3$): δ 167.5, 167.2, 161.2, 161.0, 157.1, 157.0, 154.7, 154.3, 135.6, 134.5, 132.0, 131.9, 129.7, 129.5, 127.7, 127.5, 126.0, 125.5, 120.9, 120.0, 104.3, 103.9, 99.0, 98.8, 78.4, 78.2, 76.2, 76.1, 60.4, 60.0, 55.7, 55.4, 55.3, 51.6, 51.3, 32.89, 32.86, 32.8, 23.8, 23.8, 23.7.

*N-[2-(Cyclopentylamino)-2-oxo-1-thien-2-ylethyl]-N-(3-methoxyphenyl) Propynamide (**6**).* Yield 533 mg (70%). ^{1}H NMR (400 MHz, $CDCl_3$): δ 7.23 (d, J = 5.0 Hz, 1H), 7.13 (t, J = 7.9 Hz, 1H), 6.96 (d, J = 3.3 Hz, 1H), 6.72−6.89 (m, 4H), 6.10−6.17 (m, 2H), 4.19 (sextet, J = 6.6 Hz, 1H), 3.68 (s, 3H), 2.84 (s, 1H), 1.86−2.00 (m, 2H), 1.48−1.66 (m, 4H), 1.32−1.45 (m, 2H). ^{13}C NMR (100 MHz, $CDCl_3$): δ 167.0, 159.5, 153.2, 139.8, 135.0, 129.9, 129.1, 128.0, 126.3, 122.2, 115.00, 114.97, 80.7, 75.7, 60.0, 55.2, 51.7, 32.7, 23.6, 23.5.

*N-[2-(Cyclopentylamino)-2-oxo-1-thien-2-ylethyl]-N-(2,5-dimethoxyphenyl) Propynamide (**7**).* The reaction was run in 2,2,2-trifluoroethanol (2 mL) for 1 h. Yield 207 mg (25%). In $CDCl_3$, mixture of two rotameric forms in 50:50 ratio. ^{1}H NMR (400 MHz, $CDCl_3$): δ 7.26 (br. d, J = 6.2 Hz, 0.5H), 7.21 (dd, J = 5.0 Hz, J = 1.0 Hz, 0.5H), 7.18 (dd, J = 5.0 Hz, J = 1.0 Hz, 0.5H), 7.05 (d, J = 2.9 Hz, 0.5H), 7.03 (d, J = 3.3 Hz, 0.5H), 6.94 (d, J = 3.3 Hz, 0.5H), 6.87 (dd, J = 5.4 Hz, J = 3.7 Hz, 0.5H), 6.73−6.86 (m, 4 × 0.5H), 6.69 (d, J = 9.1 Hz, 0.5H), 6.51 (br.d, J = 7.1 Hz, 0.5H), 6.18 (d, J = 2.9 Hz, 0.5H), 6.16 (s, 0.5H), 5.89 (s, 0.5H), 4.22 (sextet, J = 7.1 Hz, 0.5H), 4.20 (sextet, J = 7.1 Hz, 0.5H), 3.85 (s, 3 × 0.5H), 3.74 (s, 3 × 0.5H), 3.61 (s, 3 × 0.5H), 3.52 (s, 3 × 0.5H), 2.73 (s, 0.5H), 2.70 (s, 0.5H), 1.90−2.05 (m, 4 × 0.5H), 1.32−1.75 (m, 12 × 0.5H). ^{13}C NMR (100 MHz, $CDCl_3$): δ 167.3, 167.1, 154.2, 153.6, 153.2, 150.4, 150.2, 135.7, 134.6, 129.8, 129.5, 128.3, 127.7, 127.4, 127.2, 126.2, 125.5, 116.4, 116.2, 116.1, 115.8, 112.5, 112.0, 78.3, 78.0, 76.1, 75.9, 60.6, 60.3, 56.2, 55.8, 55.7, 55.6, 51.6, 51.2, 32.8, 32.7, 23.75, 23.71, 23.6.

*N-[2-(Cyclopentylamino)-2-oxo-1-phenylethyl]-N-(2,3-dihydro-1,4-benzodioxin-6-yl) Propynamide (**8**).* Yield 697 mg (86%). ^{1}H NMR (400 MHz, $CDCl_3$): δ 7.17−7.25 (m, 3H), 7.10−7.16 (m, 2H), 6.52−6.80 (m, 3H), 5.93 (s, 1H), 5.74 (d, J = 7.5 Hz, 1H), 4.10−4.25 (m, 5H), 2.84 (s, 1H), 1.84−2.00 (m, 2H), 1.46−1.62 (m, 4H), 1.21−1.41 (m, 2H). ^{13}C NMR (100 MHz, $CDCl_3$): δ 168.0, 153.9, 143.6, 142.8, 133.7, 132.1, 130.1, 128.6, 128.4, 123.8, 119.5, 116.5, 80.5, 76.1, 64.9, 64.1, 63.9, 51.5, 32.72, 32.67, 23.60, 23.57.

*N-[2-(Cyclopentylamino)-2-oxo-1-phenylethyl]-N-[3-methyl-4-(1H-tetraazol-1-yl)phenyl] Propynamide (**9**).* Yield 461 mg (54%). ^{1}H NMR (400 MHz, $CDCl_3$): δ 8.81 (s, 1H), 7.13−7.35 (m, 8H), 6.13 (s, 1H), 5.96 (d, J = 6.6 Hz, 1H), 4.22 (sextet, J = 6.6 Hz, 1H), 2.93 (s, 1H), 2.09 (s, 1H), 1.86−2.04 (m, 2H), 1.50−1.68 (m, 4H), 1.25−1.48 (m, 2H). ^{13}C NMR (100 MHz, $CDCl_3$): 167.9, 153.1, 142.9, 140.9, 134.4, 133.8, 133.4, 132.5, 130.1, 129.9, 129.0, 128.7, 125.5, 81.2, 75.8, 64.3, 51.7, 32.68, 32.65, 23.58, 23.56, 17.6.

*N-[2-(Cyclopentylamino)-1-(2-fluorophenyl)-2-oxoethyl]-N-(2-furylmethyl) Propynamide (**10**).* Yield 586 mg (80%). In $CDCl_3$, mixture of two rotameric forms in 70:30 ratio. ^{1}H NMR (400 MHz, $CDCl_3$): δ 7.44 (td, J = 7.5 Hz, J = 1.2 Hz, 0.7H), 7.29−7.37 (m, 2 × 0.3H), 7.22−7.29 (m, 0.7H), 7.13−7.19 (m, 2 × 0.3H+0.7H), 7.09 (td, J = 7.5 Hz, J = 1.2 Hz, 0.7H), 6.97−7.05 (m, 0.3H), 6.87−6.94 (m, 0.7H), 6.34 (s, 0.3H), 6.17 (dd, J = 2.9 Hz, J = 1.7 Hz, 0.3H), 6.09−6.14 (m, 0.3H+0.7H), 6.07 (s, 0.7H), 6.02 (br.d, J = 7.1 Hz, 0.7H), 5.95 (d, J = 3.3 Hz, 0.3H), 5.85 (d, J = 3.3 Hz, 0.7H), 4.90 (d, J = 17.0 Hz, 0.7H), 4.76 (d, J = 17.0 Hz, 0.7H), 4.61 (d, J = 15.8 Hz, 0.3H), 4.27 (d, J = 15.8 Hz, 0.3H), 4.19 (sextet, J = 7.1 Hz, 0.3H), 4.13 (sextet, J = 7.1 Hz, 0.7H), 3.26 (s, 0.3H), 3.18 (s, 0.7H), 1.85−1.99 (m, 2 × 0.3H+2 × 0.7H), 1.47−1.64 (m, 4 × 0.3H+4 × 0.7H), 1.19−1.35 (m, 2 × 0.3H+2 × 0.7H). ^{13}C NMR (100 MHz, $CDCl_3$): δ 167.4, 167.2, 161.4 (d, J = 249.8 Hz), 161.1 (d, J = 249.8 Hz), 156.3, 154.3, 154.2, 149.9, 149.8, 141.9, 141.6, 131.1, 131.0, 130.92, 130.90, 130.6 (d, J = 9.0 Hz), 124.4 (d, J = 2.6 Hz), 124.1 (d, J = 2.6 Hz), 121.3 (d, J = 14.2 Hz), 115.7 (d, J = 20.6 Hz), 115.3 (d, J = 21.9 Hz), 110.6, 110.3, 108.7, 108.0, 80.9, 80.0, 75.5, 74.8, 60.4, 55.23, 55.21, 51.5, 51.4, 44.6, 39.4, 32.64, 32.60, 23.6. ^{19}F NMR (376 MHz, $CDCl_3$): −114.62 (0.3F), −114.75 (0.7F).

*N-[2-(Cyclopentylamino)-1-(4-methoxyphenyl)-2-oxoethyl]-N-(3,5-dimethoxyphenyl) Propynamide (**11**).* Yield 62 mg (7%). ^{1}H NMR (400 MHz, $CDCl_3$): δ 7.04−7.14 (m, 2H), 6.70−6.77 (m, 2H), 6.30−6.45 (m, 3H), 5.86 (s, 1H), 5.53 (br.d, J = 7.1 Hz, 1H), 4.20 (sextet, J = 6.6 Hz, 1H), 3.74 (s, 3H), 3.64 (s, 6H), 2.83 (s, 1H), 1.85−2.02 (m, 2H), 1.47−1.63 (m, 4H), 1.21−1.41 (m, 2H). ^{13}C NMR (100 MHz, $CDCl_3$): δ 168.2, 160.2, 159.7, 153.4, 140.6, 131.5, 125.6, 113.8, 108.7, 101.2, 80.1, 76.1, 64.6, 55.4, 55.2, 51.6, 32.8, 32.7, 23.62, 23.60.

*N-[2-(Cyclopentylamino)-1-(4-fluorophenyl)-2-oxoethyl]-N-[3-(trifluoromethyl)phenyl] Propynamide (**12**).* Yield 522 mg (60%). ^{1}H NMR (400 MHz, $CDCl_3$): δ 7.24−7.54 (m, 4H), 7.09 (dd, J = 8.7 Hz, J = 5.4 Hz, 2H), 6.88 (t, J = 8.7 Hz, 2H), 6.09 (s, 1H), 5.87 (br.s, 1H), 4.21 (sextet, J = 7.1 Hz, 1H), 2.83 (s, 1H), 1.79−2.05 (m, 2H), 1.48−1.68 (m, 4H), 1.35−1.47 (m, 1H), 1.21−1.32 (m, 1H). ^{13}C NMR (100 MHz, $CDCl_3$): δ 167.9, 162.8 (d, J = 249.8 Hz), 153.4, 138.9, 134.7, 132.1 (d, J = 9.0 Hz), 130.8 (quartet, J = 33.5 Hz), 129.1 (d, J = 2.6 Hz), 129.0, 128.1 (quartet, J = 3.9 Hz), 125.3 (quartet, J = 3.9 Hz), 123.3 (quartet, J = 271.7 Hz), 115.6 (d, J = 20.6 Hz), 81.3, 75.5, 63.3, 51.7, 31.73, 32.71, 23.63, 23.59. ^{19}F NMR (376 MHz, $CDCl_3$): δ −62.80, −111.77.

*N-[2-(Cyclohexylamino)-2-oxo-1-thien-2-ylethyl]-N-[3-(trifluoromethyl) phenyl] Propynamide (**13**).* Yield 579 mg (67%). ^{1}H NMR (400 MHz, $CDCl_3$): δ 7.46−7.55 (m, 2H), 7.35−7.43 (m, 2H), 7.23 (dd, J = 5.0 Hz, J = 0.8 Hz, 1H), 6.92 (d, J = 3.3 Hz, 1H), 6.85 (dd, J = 5.0 Hz, J = 3.3 Hz, 1H), 6.25 (s, 1H), 6.16 (br.d, J = 7.1 Hz, 1H), 4.20 (sextet, J = 6.7 Hz, 1H), 2.85 (s, 1H), 1.87−2.03 (m, 2H), 1.50−1.67 (m, 4H), 1.31−1.46 (m, 2H). ^{13}C NMR (100 MHz, $CDCl_3$): δ 167.0, 153.0, 139.1, 134.5, 134.0, 131.9 (quartet, J = 33.5 Hz), 130.1, 129.1, 128.2, 127.4 (quartet, J = 3.9 Hz), 126.6, 125.4 (quartet, J = 3.9 Hz), 123.3 (quartet, J = 273.0 Hz), 81.4, 75.4, 59.3, 51.8, 32.7, 23.63, 23.58. ^{19}F NMR (376 MHz, $CDCl_3$): δ −62.69.

*N-[2-(Cyclopentylamino)-2-oxo-1-phenylethyl]-N-(2-naphthyl) Propynamide (**14**).* Yield 652 mg (82%). ^{1}H NMR (400 MHz, DMSO-d_6): δ 8.24 (d, J = 6.6 Hz, 1H), 7.88 (br.s, 1H), 7.74−7.84 (m, 2H), 7.60−7.73 (m, 1H), 7.40−7.50 (m, 2H), 6.99−7.17 (m, 5H), 6.10 (s, 1H), 4.11 (s, 1H), 4.08 (sextet, J = 6.6 Hz, 1H), 1.71−1.90 (m, 2H), 1.38−1.68 (m, 5H), 1.21−1.33 (m, 1H). ^{13}C NMR (100 MHz, DMSO-d_6): δ 168.2, 152.8, 136.2, 134.3, 132.2, 131.9, 130.01, 129.96, 128.7,

127.9, 127.4, 127.3, 126.5, 126.2, 83.1, 76.8, 63.6, 50.7, 32.1, 31.8, 23.44, 23.40.

*N-(1,3-Benzodioxol-5-ylmethyl)-N-[2-(benzylamino)-1-(2-fluorophenyl)-2-oxoethyl] Propynamide (**15**).* Yield 814 mg (92%). In DMSO-d_6, mixture of two rotameric forms in 60:40 ratio. ^{1}H NMR (400 MHz, DMSO-d_6): δ 8.99 (t, J = 5.8 Hz, 0.4H), 8.85 (t, J = 5.8 Hz, 0.6H), 7.22−7.38 (m, 6H), 7.18 (td, J = 7.5 Hz, J = 1.2 Hz, 0.4H), 7.11 (td, J = 7.5 Hz, J = 1.2 Hz, 0.6H), 6.97−7.03 (m, 0.4H), 6.84−6.91 (m, 0.6H), 6.63 (d, J = 7.9 Hz, 0.6H), 6.57 (d, J = 7.9 Hz, 0.4H), 6.46 (s, 0.4H), 6.42 (d, J = 1.2 Hz, 0.6H), 6.34 (dd, J = 7.9 Hz, J = 1.2 Hz, 0.6H), 6.28 (d, J = 1.2 Hz, 0.4H), 6.25 (s, 0.6H), 6.19 (dd, J = 7.9 Hz, J = 1.2 Hz, 0.4H), 5.88−5.95 (m, 2 × 0.6H+2 × 0.4H), 5.07 (d, J = 17.0 Hz, 0.6H), 4.93 (d, J = 15.8 Hz, 0.4H), 4.81 (s, 0.4H), 4.62 (s, 0.6H), 4.51 (d, J = 17.0 Hz, 0.6H), 4.26−4.44 (m, 2 × 0.6H+2 × 0.4H), 4.15 (d, J = 15.8 Hz, 0.4H). ^{13}C NMR (100 MHz, DMSO-d_6): δ 168.6, 161.4 (d, J = 247.2 Hz), 161.2 (d, J = 247.2 Hz), 154.7, 154.6, 151.7, 147.1, 147.0, 146.2, 146.0, 139.3, 139.2, 131.7, 131.56, 131.48, 131.40, 131.37, 131.32, 130.88, 130.86, 130.62, 130.60, 128.8, 128.7, 127.8, 127.7, 127.4, 127.3, 124.9 (d, J = 2.6 Hz), 124.7 (d, J = 2.6 Hz), 122.9 (d, J = 14.2 Hz), 122.3 (d, J = 14.2 Hz), 120.5, 119.7, 115.6 (d, J = 20.6 Hz), 115.3 (d, J = 20.6 Hz), 108.0, 107.9, 107.7, 106.9, 101.2, 101.1, 84.2, 83.1, 76.7, 75.9, 59.0, 54.5, 50.6, 47.4, 43.0, 42.8. ^{19}F NMR (376 MHz, DMSO-d_6): δ −114.70 (0.6F), −115.24 (0.4F).

*N-[2-(Benzylamino)-2-oxo-1-thien-2-ylethyl]-N-[3-(trifluoromethyl)-phenyl] Propynamide (**16**).* Yield 498 mg (56%). ^{1}H NMR (400 MHz, $CDCl_3$): δ 7.58 (d, J = 7.5 Hz, 1H), 7.53 (br.d, J = 7.9 Hz, 1H), 7.47 (br. s, 1H), 7.41 (t, J = 7.9 Hz, 1H), 7.22−7.35 (m, 6H), 6.95 (d, J = 3.3 Hz, 1H), 6.87 (dd, J = 5.0 Hz, J = 3.7 Hz, 1H), 6.78 (br.t, J = 5.4 Hz, 1H), 6.33 (s, 1H), 4.42−4.54 (m, 2H), 2.88 (s, 1H). ^{13}C NMR (100 MHz, $CDCl_3$): δ 127.6, 153.0, 139.1, 137.6, 134.2, 133.9, 130.9 (quartet, J = 33.5 Hz), 130.3, 129.1, 128.5, 128.3, 127.39, 127.35, 127.30, 127.26, 126.6, 125.4 (quartet, J = 3.9 Hz), 123.3 (quartet, J = 273.0 Hz), 81.4, 75.3, 59.6, 43.7. ^{19}F NMR (376 MHz, $CDCl_3$): δ −62.57.

*N-(2-Chlorobenzyl)-N-[2-(cyclopentylamino)-2-oxo-1-phenylethyl] Propynamide (**17**).* Yield 482 mg (61%). In $CDCl_3$, mixture of two rotameric forms in 80:20 ratio. ^{1}H NMR (400 MHz, $CDCl_3$): δ 7.05−7.33 (m, 9 × 0.8H+6 × 0.2H), 6.97−7.03 (m, 2 × 0.2H), 6.87−6.92 (m, 0.2H), 6.21 (s, 0.2H), 6.06 (br.d, J = 7.5 Hz, 0.2H), 5.99 (br.d, J = 7.1 Hz, 0.8H), 5.78 (s, 0.8H), 5.14 (d, J = 17.9 Hz, 0.8H), 4.95 (d, J = 17.0 Hz, 0.2H), 4.93 (d, J = 17.9 Hz, 0.8H), 4.64 (d, J = 17.0 Hz, 0.2H), 4.12−4.28 (m, 0.8H+0.2H), 3.40 (s, 0.2H), 3.04 (s, 0.8H), 1.87−1.99 (m, 2 × 0.8H+2 × 0.2H), 1.49−1.65 (m, 4 × 0.8H+4 × 0.2H), 1.27−1.40 (m, 2 × 0.8H+2 × 0.2H). ^{13}C NMR (100 MHz, $CDCl_3$): δ 167.6, 167.5, 155.0, 154.4, 134.1, 133.7, 133.5, 131.9, 131.8, 129.4, 129.17, 128.88, 128.71, 128.62, 128.56, 128.02, 127.7, 127.6, 126.3, 126.2, 81.0, 79.6, 75.5, 75.4, 66.0, 62.2, 51.5, 51.4, 48.9, 45.1, 32.6, 32.5, 23.57, 23.54.

*N-[2-(Cyclohexylamino)-2-oxo-1-thien-2-ylethyl]-N-phenyl Propynamide (**18**).* Yield 487 mg (66%). ^{1}H NMR (400 MHz, $CDCl_3$): δ 7.16−7.35 (m, 6H), 6.97 (d, J = 2.9 Hz, 1H), 6.85−6.91 (m, 1H), 6.24 (s, 1H), 6.15 (br.d, J = 7.9 Hz, 1H), 3.75−3.87 (m, 1H), 2.84 (s, 1H), 1.83−1.99 (m, 2H), 1.53−1.75 (m, 3H), 1.27−1.43 (m, 2H), 1.08−1.25 (m, 3H). ^{13}C NMR (100 MHz, $CDCl_3$): δ 166.6, 153.3, 138.7, 134.9, 130.0, 129.8, 128.8, 128.5, 127.9, 126.2, 80.8, 75.7, 59.7, 48.7, 32.5, 32.4, 25.3, 24.6, 24.5.

*N-[2-(Cyclohexylamino)-1-(2-fluorophenyl)-2-oxoethyl]-N-(2-fluorophenyl) Propynamide (**19**).* Yield 548 mg (69%). In $CDCl_3$, mixture of two rotameric forms in 75:25 ratio. ^{1}H NMR (400 MHz, $CDCl_3$): δ 7.91 (td, J = 7.9 Hz, J = 1.7 Hz, 0.75H), 7.31 (br.t, J = 7.9 Hz, 0.25H), 7.10−7.25 (m, 2 × 0.75H+2 × 0.25H), 6.84−7.09 (m, 3 × 0.75H+3 × 0.25H), 6.68−6.82 (m, 2 × 0.75H+2 × 0.25H), 6.40−6.47 (m, 0.75H+0.25H), 6.15 (s, 0.25H), 6.09 (br.d, J = 7.9 Hz, 0.75H), 3.70−3.82 (m, 0.75H+0.25H), 2.80 (s, 0.25H), 2.71 (s, 0.75H), 1.49−1.98 (m, 5 × 0.75H+5 × 0.25H), 0.94−1.37 (m, 5 × 0.75H+5 × 0.25H). ^{13}C NMR (100 MHz, $CDCl_3$): δ 167.2, 165.9, 161.0 (d, J = 249.8 Hz), 160.8 (d, J = 248.5 Hz), 159.2 (d, J = 249.8 Hz), 159.1 (d, J = 251.1 Hz), 153.8, 153.6, 133.2, 131.7, 131.5, 131.2, 130.8, 130.7, 130.65, 130.57, 126.4 (d, J = 11.6 Hz), 126.0 (d, J = 12.9 Hz), 124.1, 124.0 (d, J = 3.9 Hz), 123.4 (d, J = 3.9 Hz), 121.3 (d, J = 14.2 Hz), 120.1 (d, J = 14.2 Hz), 115.9 (d, J = 20.6 Hz), 115.2 (d, J = 20.6 Hz), 79.9, 79.2, 75.4, 75.1, 58.58, 58.56, 56.67, 56.64, 48.9, 48.4, 32.48, 32.44, 25.33, 25.27, 24.7, 24.6, 24.52, 24.48. ^{19}F NMR (376 MHz, $CDCl_3$): δ −114.95 (0.75F+0.25F), −118.16 (0.25F), −119.47 (0.75F).

Computational Simulation to Predict the Drug-like Properties of PACMA Compounds. After the required ligand structures of a specified configuration were built, energy minimization was performed using the Catalyst software package (Accelrys, Inc., San Diego, CA). The lowest-energy conformation for each compound was exported to ADMET Predictor to calculate ADME (absorption, distribution, metabolism, and excretion) properties and 3-D polar surface areas.

Cell Culture. The human breast cancer cell line MDA-MB-435 and the colon cancer cell line HT29 were purchased from the American Type Cell Culture (Manassas, VA). Colon cancer cell lines HCT116 p53$^{+/+}$ and HCT116 p53$^{-/-}$ were kindly provided by Dr. Bert Vogelstein (Johns Hopkins Medical Institutions, Baltimore, MD). The human ovarian carcinoma cell line (HEY), naturally resistant to cisplatin (CDDP), was kindly provided by Dr. Louis Dubeau (USC Norris Cancer Center).[41,42] The bladder cancer cell lines were kindly provided by Dr. Richard Cote (USC Keck School of Medicine). Cells were maintained as monolayer cultures in the appropriate media: RPMI-1640 (HT29, HCT116 p53$^{+/+}$, HCT116 p53$^{-/-}$, and HEY cell lines) or DMEM (MDA-MB-435 and UMUC3 cell lines) supplemented with 10% fetal bovine serum (FBS) (HyClone, Road Logan, UT) at 37 °C in a humidified atmosphere of 5% CO_2. To remove the adherent cells from the flask for subculture and counting, cells were washed with PBS without calcium or magnesium, incubated with a small volume of 1× trypsin−EDTA solution (Sigma-Aldrich, St. Louis, MO) for 5 min, resuspended with fresh culture medium, and centrifuged at 1200 rpm for 5 min. All experiments were performed using cells in exponential growth phase. Cells were routinely checked for *Mycoplasma* contamination using PlasmoTest kit (InvivoGen, San Diego, CA).

Compound Dilutions. Ten millimolar stock solutions of all compounds were prepared in DMSO and stored at −20 °C. Further dilutions were made fresh in cell-culture media.

Cytotoxicity Assays. Cytotoxicity was assessed by MTT assay as described previously.[43] In brief, cells were seeded in 96-well microtiter plates and allowed to attach overnight. Cells were subsequently treated with continuous exposure to corresponding drugs for 72 h. At the end of treatments, an MTT solution (at a final concentration of 0.5 mg/mL) was added to each well, and cells were incubated for 4 h at 37 °C. After removal of the supernatant, DMSO was added, and the absorbance was read at 570 nm. All assays were done in triplicate. The IC_{50} was then determined for each drug from a plot of log(drug concentration) versus percentage of cells killed.

Colony Formation Assay. Colony formation assays were performed as previously described to confirm the activity of these compounds.[44] In brief, cells were plated in 24-well plates at a density of 1000 cells per well and allowed to attach overnight. The next day, 1 μM concentration of each compound was added for 24 h. Cells were washed with 1× PBS, and fresh media was then added to the cells. Cells were incubated until colonies formed (8−10 days). Subsequently, cells were washed, fixed with a 1% glutaraldehyde solution for 30 min, and stained with a solution of crystal violet (2%) for 30 min. After staining, cells were thoroughly washed with distilled water. Colonies were imaged on a Chemi-Doc Imaging System (Bio-Rad, Hercules, CA) and counted using the Quantity One software package (Bio-Rad, Hercules, CA). The data reported is a representative of at least three independent experiments.

***In Vivo* Mouse Xenograft Studies.** Sixteen virgin female athymic nude (*nu/nu*) mice (Simonsen Laboratory Inc., Gilroy, CA) were used for *in vivo* efficacy testing. The animals were fed *ad libitum* and kept in temperature controlled rooms at 20 ± 2 °C with a 12 h light−dark period. Animal care and manipulation were in agreement with the University of Southern California (USC) institutional guidelines, which are in accordance with the Guidelines for the Care and Use of Laboratory Animals.

Human breast cancer MDA-MB-435 cells in logarithmic phase growth from *in vitro* cell culture were inoculated subcutaneously on the rear flank of the mice (1.5×10^6 cells/mouse) under aseptic conditions. Tumor growth was assessed twice weekly by measuring tumor diameters with a Vernier caliper (length × width). Tumor weight was calculated according to the formula: TW (mg) = tumor volume (mm^3) = $d^2 \times D/2$, where d and D are the shortest and longest diameters, respectively. Tumors were allowed to grow to an average volume of 100 mm^3. Animals were then randomly assigned to control and treatment groups ($n = 8$), to receive vehicle control or compound **2** (10 mg/kg for 9 days, 20 mg/kg for 5 days, and 40 mg/kg for 12 days, **2** was dissolved in 10% DMSO/90% sesame oil) via i.p. injection once daily. Treatment of each animal was based on the average body weight of the treatment group.

Statistical Analysis. Eight mice were assigned to each group and the results were expressed as the mean ± SEM. Statistical analysis and p-value determination were done by two-tailed paired t-test with a confidence interval of 95% for determination of the differences between groups. A p-value of <0.05 was considered to be statistically significant. ANOVA was used to test for significance among groups. The SAS statistical software package (SAS Institute, Cary, NC) was used for statistical analysis.

Cell Cycle Analysis. Cell cycle perturbations were analyzed by propidium iodide DNA staining. Exponentially growing MDA-MB-435 cells were treated with 5 μM compound **4** for 6, 12, and 24 h. At the end of treatment, cells were collected and washed with 1× PBS after a gentle centrifugation at 1500 rpm for 5 min. Cells were then thoroughly resuspended in 0.5 mL of PBS and fixed in 70% ethanol overnight at 4 °C. Ethanol-fixed cells were centrifuged at 3000 rpm for 5 min and washed twice in PBS to remove residual ethanol. For cell cycle analysis, the pellets were resuspended in 1 mL of PBS containing 0.02 mg/mL of propidium iodide and 0.5 mg/mL of DNase-free RNase A and incubated at 37 °C for 30 min. Cell cycle profiles were obtained using a BD LSRII flow cytometer (BD Biosciences, San Jose, CA). Propidium iodide was excited using a 488 nm blue argon laser. Resulting fluorescence was measured using a PMT detector equipped with 550 nm long pass dichroic mirror and 575/26 bandpass filter. Data were analyzed with the ModFit LT software package (Verify Software House, Inc., Topsham, ME).

Apoptosis Assay. To quantify drug-induced apoptosis, annexin V/propidium iodide staining was performed and analyzed by flow cytometry. MDA-MB-435 cells were treated with 10 μM compound **1**, **2**, or **4** for 24 and 48 h. After treatment, both floating and adherent cells were combined and subjected to annexin V/propidium iodide staining using an annexin V−FITC apoptosis detection kit (Oncogene Research Products, San Diego, CA) according to manufacturer's recommendations. Untreated control cells (48 h) were maintained in parallel to drug-treated groups. Double staining was used to distinguish between viable, early apoptotic, and necrotic or late apoptotic cells. The resulting fluorescence (FITC-A channel for green fluorescence and PE-A channel for red fluorescence) was measured by flow cytometry using a BD LSRII flow cytometer (BD Biosciences, San Jose, CA). According to this method, the lower left quadrant shows the viable cells, the upper left quadrant shows early apoptotic cells, the upper right quadrant shows late apoptotic, and the lower right quadrant shows both necrotic cells and cellular debris.

Western Blotting Analysis. Cells were detached using 1× trypsin−EDTA solution and collected by centrifugation at 1200 rpm for 5 min. Cells were then lysed in 80 μL of 1× cell lysis buffer (50 mM Tris-HCl, pH 7.5, 150 mM NaCl, and 1% NP-40) and pelleted by centrifugation at 14 000 rpm for 20 min at 4 °C. Protein concentration of the whole cell lysates was measured using BCA protein assay and equal amounts of total protein were resolved on a 10% tris-glycine gel via SDS−PAGE. The separated proteins were electroblotted onto nitrocellulose membrane and blocked in 5% BSA/PBS for 1 h at room temperature. The membrane was probed with anti-p53 (SC-126, Santa Cruz Biotechnology Inc.), anticaspase 9 (Cat. no. 9508; Cell Signaling Technology), anti-α-tubulin (SC-5286, Santa Cruz Biotechnology Inc.), and anti-GAPDH (Y3322GAPDH, Biochain Institute, Inc.) antibodies at 4 °C overnight. Horseradish peroxidase-conjugated secondary antibodies (Invitrogen, Carlsbad, CA) in combination with SuperSignal Dura (ThermoFisher, Rockford, IL) enhanced chemiluminescence (ECL) solutions were used to visualize proteins of interest with a ChemiDoc Imaging system (Bio-Rad, Hercules, CA).

Kinexus Antibody Microarray. MDA-MB-435 cells were treated with 0.1 μM compound **1** for 24 h. After treatment, cells were washed with ice-cold PBS to remove residual medium. Cells were then lysed in 200 μL of lysis buffer (20 mM MOPS, pH 7.0, 2 mM EGTA, 5 mM EDTA, 30 mM sodium fluoride, 60 mM β-glycerophosphate, pH 7.2, 20 mM sodium pyrophosphate, 1 mM sodium orthovanadate, 1 mM phenylmethylsulfonylfluoride, 3 mM benzamidine, 5 μM pepstatin A, 10 μM leupeptin, 1% Triton X-100, 1 mM dithiothreitol) and collected into a microcentrifuge tube. The cell lysates were sonicated four times for 10 s each with 15 s intervals on ice to rupture cell membrane and shear chromosomal DNA. After sonication, the homogenates were centrifuged at 90 000 × g for 30 min at 4 °C. The supernatants were then transferred to a clean microcentrifuge tube, and the protein concentrations were measured using BCA protein assay. Aliquots (250 μL) of the whole cell lysates were submitted to Kinexus for the 628-antibody microarray analysis.

Ingenuity Pathway Analysis. Potential signaling pathways induced by compound **1** were analyzed by Ingenuity Pathway Analysis (IPA) software using the Kinexus 628-antibody microarray results. The statistically significant up-regulated or down-regulated pan-specific proteins with their corresponding Swiss-Prot accession numbers and ratio changes were uploaded as an Excel spreadsheet file to the IPA server. Compound **1**-mediated signaling pathways were then analyzed by IPA core analysis.

Detection of Mitochondrial Superoxide Production. MDA-MB-435 cells were treated with compounds **1**, **2**, **4**, and **18** at their IC_{50} or 3 × IC_{50} for 24 h. After drug treatments, a solution of 5 μM MitoSOX Red mitochondrial superoxide indicator (Invitrogen, Carlsbad, CA) was added, and cells were incubated for 10 min at 37 °C. Cells were then washed three times with Hank's balanced salt solution (HBSS) to remove excess MitoSOX. After washing, cells were either observed under the fluorescence microscope or collected by trypsinization, washed twice with HBSS, and measured for superoxide production using a BD LSRII flow cytometer (BD Biosciences, San Jose, CA, USA). Data were analyzed with the BD FACSDiva software package (BD Biosciences, San Jose, CA, USA).

Pharmacokinetics Study. Preliminary pharmacokinetics of compounds **4** and **9** were performed using 18 mice, each time point consisting of two mice. Mice were stratified to various doses given as an i.p. injection of **4** and **9** (24 mg/kg). At the specified time points following drug administration, blood was collected with heparinized syringes. The samples were allowed to settle in 500 μL eppendorf vials and then centrifuged at 1500 rpm for 10 min. The plasma was removed, transferred into new eppendorf tube, and frozen at −80 ° C until analysis.

■ ASSOCIATED CONTENT

Ⓢ Supporting Information. Structures, colony formation assay for moderately active and inactive compounds, and selected

properties of all eight cell lines. This material is available free of charge via the Internet at http://pubs.acs.org.

AUTHOR INFORMATION

Corresponding Author

*Mailing adress: Department of Pharmacology and Pharmaceutical Sciences, University of Southern California, Los Angeles, California, 90089. Phone: 323-442-2341. Fax: 323-442-1390. E-mail: neamati@usc.edu.

ACKNOWLEDGMENT

This study was supported in part by the Sharon and William Cockrell Endowed Cancer Research Fund (N.N.) and by the USC Zumberge Research and Innovation Fund (N.A.P.).

ABBREVIATIONS

ADMET, absorption, distribution, metabolism, excretion, and toxicity; DCFH, 2,7-dichlorodihydrofluorescein; DMSO, dimethyl sulfoxide; HBA, hydrogen-bond acceptor; HBD, hydrogen-bond donor; HSP, heat shock protein; HTS, high-throughput screening; i.p., intraperitoneal; IPA, Ingenuity Pathway Analysis; MMA, monomethylarsonous acid; MW, molecular weight; MLogP, Moriguchi octanol−water partition coefficient; Nrf2, nuclear factor erythroid 2-related factor 2; PACMAs, propynoic acid carbamoyl methyl amides; PBS, phosphate-buffered saline; PK, pharmacokinetics; PD, pharmacodynamics; PSA, polar surface area, three-dimensional; ROS, reactive oxygen species; SAR, structure−activity relationship; SEM, standard error of mean; SOD1, superoxide dismutase 1; S+ logP), SimulationsPlus, Inc., model of log P

REFERENCES

(1) Dy, G. K.; Adjei, A. A. Systemic cancer therapy: evolution over the last 60 years. *Cancer* **2008**, *113*, 1857–1887.

(2) Kummar, S.; Chen, H. X.; Wright, J.; Holbeck, S.; Millin, M. D.; Tomaszewski, J.; Zweibel, J.; Collins, J.; Doroshow, J. H. Utilizing targeted cancer therapeutic agents in combination: Novel approaches and urgent requirements. *Nat. Rev. Drug Discovery* **2010**, *9*, 843–856.

(3) Neamati, N.; Barchi, J. J., Jr. New paradigms in drug design and discovery. *Curr. Top. Med. Chem.* **2002**, *2*, 211–227.

(4) Loging, W.; Harland, L.; Williams-Jones, B. High-throughput electronic biology: Mining information for drug discovery. *Nat. Rev. Drug Discovery* **2007**, *6*, 220–230.

(5) Lamb, J. The Connectivity Map: A new tool for biomedical research. *Nat. Rev. Cancer* **2007**, *7*, 54–60.

(6) Akritopoulou-Zanze, I. Isocyanide-based multicomponent reactions in drug discovery. *Curr. Opin. Chem. Biol.* **2008**, *12*, 324–331.

(7) Akritopoulou-Zanze, I.; Djuric, S. W. Recent advances in the development and applications of post-ugi transformations. *Heterocycles* **2007**, *73*, 125–147.

(8) Domling, A. Recent developments in isocyanide based multicomponent reactions in applied chemistry. *Chem. Rev.* **2006**, *106*, 17–89.

(9) Lipinski, C. A. Drug-like properties and the causes of poor solubility and poor permeability. *J. Pharmacol. Toxicol. Methods* **2000**, *44*, 235–249.

(10) Lipinski, C. A.; Lombardo, F.; Dominy, B. W.; Feeney, P. J. Experimental and computational approaches to estimate solubility and permeability in drug discovery and development settings. *Adv. Drug Delivery Rev.* **2001**, *46*, 3–26.

(11) Palm, K.; Luthman, K.; Ungell, A. L.; Strandlund, G.; Artursson, P. Correlation of drug absorption with molecular surface properties. *J. Pharm. Sci.* **1996**, *85*, 32–39.

(12) Palm, K.; Stenberg, P.; Luthman, K.; Artursson, P. Polar molecular surface properties predict the intestinal absorption of drugs in humans. *Pharm. Res.* **1997**, *14*, 568–571.

(13) Palm, K.; Luthman, K.; Ungell, A. L.; Strandlund, G.; Beigi, F.; Lundahl, P.; Artursson, P. Evaluation of dynamic polar molecular surface area as predictor of drug absorption: comparison with other computational and experimental predictors. *J. Med. Chem.* **1998**, *41*, 5382–5392.

(14) Kelder, J.; Grootenhuis, P. D.; Bayada, D. M.; Delbressine, L. P.; Ploemen, J. P. Polar molecular surface as a dominating determinant for oral absorption and brain penetration of drugs. *Pharm. Res.* **1999**, *16*, 6.

(15) Alvarez, M.; Paull, K.; Monks, A.; Hose, C.; Lee, J. S.; Weinstein, J.; Grever, M.; Bates, S.; Fojo, T. Generation of a drug resistance profile by quantitation of mdr-1/P-glycoprotein in the cell lines of the National Cancer Institute Anticancer Drug Screen. *J. Clin. Invest.* **1995**, *95*, 2205–2214.

(16) Lee, J. S.; Paull, K.; Alvarez, M.; Hose, C.; Monks, A.; Grever, M.; Fojo, A. T.; Bates, S. E. Rhodamine efflux patterns predict P-glycoprotein substrates in the National Cancer Institute drug screen. *Mol. Pharmacol.* **1994**, *46*, 627–638.

(17) Sanchez-Carbayo, M.; Socci, N. D.; Charytonowicz, E.; Lu, M.; Prystowsky, M.; Childs, G.; Cordon-Cardo, C. Molecular profiling of bladder cancer using cDNA microarrays: Defining histogenesis and biological phenotypes. *Cancer Res.* **2002**, *62*, 6973–6980.

(18) Dehnavi, E.; Soheili, Z. S.; Samiei, S.; Ataei, Z.; Aryan, H. The effect of TGF-beta2 on MMP-2 production and activity in highly metastatic human bladder carcinoma cell line 5637. *Cancer Invest.* **2009**, *27*, 568–5674.

(19) Arima, Y.; Inoue, Y.; Shibata, T.; Hayashi, H.; Nagano, O.; Saya, H.; Taya, Y. Rb depletion results in deregulation of E-cadherin and induction of cellular phenotypic changes that are characteristic of the epithelial-to-mesenchymal transition. *Cancer Res.* **2008**, *68*, 5104–5112.

(20) Schnier, J. B.; Nishi, K.; Goodrich, D. W.; Bradbury, E. M. G1 arrest and down-regulation of cyclin E/cyclin-dependent kinase 2 by the protein kinase inhibitor staurosporine are dependent on the retinoblastoma protein in the bladder carcinoma cell line 5637. *Proc. Natl. Acad. Sci. U.S.A.* **1996**, *93*, 5941–5946.

(21) Lowe, S. W.; Lin, A. W. Apoptosis in cancer. *Carcinogenesis* **2000**, *21*, 485–495.

(22) Assuncao Guimaraes, C.; Linden, R. Programmed cell deaths. Apoptosis and alternative deathstyles. *Eur. J. Biochem.* **2004**, *271*, 1638–1650.

(23) Pommier, Y.; Sordet, O.; Antony, S.; Hayward, R. L.; Kohn, K. W. Apoptosis defects and chemotherapy resistance: Molecular interaction maps and networks. *Oncogene* **2004**, *23*, 2934–2949.

(24) Norbury, C. J.; Zhivotovsky, B. DNA damage-induced apoptosis. *Oncogene* **2004**, *23*, 2797–2808.

(25) Zhang, J. Y. Apoptosis-based anticancer drugs. *Nat. Rev. Drug Discovery* **2002**, *1*, 101–102.

(26) Schuler, M.; Bossy-Wetzel, E.; Goldstein, J. C.; Fitzgerald, P.; Green, D. R. p53 induces apoptosis by caspase activation through mitochondrial cytochrome c release. *J. Biol. Chem.* **2000**, *275*, 7337–7342.

(27) Ding, H. F.; McGill, G.; Rowan, S.; Schmaltz, C.; Shimamura, A.; Fisher, D. E. Oncogene-dependent regulation of caspase activation by p53 protein in a cell-free system. *J. Biol. Chem.* **1998**, *273*, 28378–28383.

(28) Kobayashi, M.; Yamamoto, M. Molecular mechanisms activating the Nrf2-Keap1 pathway of antioxidant gene regulation. *Antioxid. Redox Signaling* **2005**, *7*, 385–394.

(29) Zhang, D. D. The Nrf2-Keap1-ARE signaling pathway: The regulation and dual function of Nrf2 in cancer. *Antioxid. Redox Signaling* **2010**, *13*, 1623–1626.

(30) Giudice, A.; Arra, C.; Turco, M. C. Review of molecular mechanisms involved in the activation of the Nrf2-ARE signaling pathway by chemopreventive agents. *Methods Mol. Biol.* **2010**, *647*, 37–74.

(31) Aleksunes, L. M.; Manautou, J. E. Emerging role of Nrf2 in protecting against hepatic and gastrointestinal disease. *Toxicol. Pathol.* **2007**, *35*, 459–473.

(32) Wasserman, W. W.; Fahl, W. E. Functional antioxidant responsive elements. *Proc. Natl. Acad. Sci. U.S.A.* **1997**, *94*, 5361–5366.

(33) Rushmore, T. H.; Morton, M. R.; Pickett, C. B. The antioxidant responsive element. Activation by oxidative stress and identification of the DNA consensus sequence required for functional activity. *J. Biol. Chem.* **1991**, *266*, 11632–11639.

(34) Friling, R. S.; Bensimon, A.; Tichauer, Y.; Daniel, V. Xenobiotic-inducible expression of murine glutathione S-transferase Ya subunit gene is controlled by an electrophile-responsive element. *Proc. Natl. Acad. Sci. U.S.A.* **1990**, *87*, 6258–6262.

(35) Chen, C. W.; Chang, Y. H.; Tsi, C. J.; Lin, W. W. Inhibition of IFN-gamma-mediated inducible nitric oxide synthase induction by the peroxisome proliferator-activated receptor gamma agonist, 15-deoxy-delta 12,14-prostaglandin J2, involves inhibition of the upstream Janus kinase/STAT1 signaling pathway. *J. Immunol.* **2003**, *171*, 979–988.

(36) Kwak, M. K.; Wakabayashi, N.; Itoh, K.; Motohashi, H.; Yamamoto, M.; Kensler, T. W. Modulation of gene expression by cancer chemopreventive dithiolethiones through the Keap1-Nrf2 pathway. Identification of novel gene clusters for cell survival. *J. Biol. Chem.* **2003**, *278*, 8135–8145.

(37) Zhang, L.; Nephew, K. P.; Gallagher, P. J. Regulation of death-associated protein kinase. Stabilization by HSP90 heterocomplexes. *J. Biol. Chem.* **2007**, *282*, 11795–11804.

(38) Pespeni, M. H.; Hodnett, M.; Abayasiriwardana, K. S.; Roux, J.; Howard, M.; Broaddus, V. C.; Pittet, J. F. Sensitization of mesothelioma cells to tumor necrosis factor-related apoptosis-inducing ligand-induced apoptosis by heat stress via the inhibition of the 3-phosphoinositide-dependent kinase 1/Akt pathway. *Cancer Res.* **2007**, *67*, 2865–2871.

(39) Shen, S. C.; Yang, L. Y.; Lin, H. Y.; Wu, C. Y.; Su, T. H.; Chen, Y. C. Reactive oxygen species-dependent HSP90 protein cleavage participates in arsenical As(+3)- and MMA(+3)-induced apoptosis through inhibition of telomerase activity via JNK activation. *Toxicol. Appl. Pharmacol.* **2008**, *229*, 239–251.

(40) Gaponik, P. N.; Karavai, V. P.; Davshko, I. E.; Degtyarik, M. M.; Bogatikov, A. N. Synthesis and properties of phenylenebis-1H-tetrazoles. *Chem. Heterocycl. Compd.* **1990**, *26*, 1274–1278.

(41) Buick, R. N.; Pullano, R.; Trent, J. M. Comparative properties of five human ovarian adenocarcinoma cell lines. *Cancer Res.* **1985**, *45*, 3668–3676.

(42) Hamaguchi, K.; Godwin, A. K.; Yakushiji, M.; O'Dwyer, P. J.; Ozols, R. F.; Hamilton, T. C. Cross-resistance to diverse drugs is associated with primary cisplatin resistance in ovarian cancer cell lines. *Cancer Res.* **1993**, *53*, 5225–5232.

(43) Carmichael, J.; DeGraff, W. G.; Gazdar, A. F.; Minna, J. D.; Mitchell, J. B. Evaluation of a tetrazolium-based semiautomated colorimetric assay: Assessment of chemosensitivity testing. *Cancer Res.* **1987**, *47*, 936–942.

(44) Munshi, A.; Hobbs, M.; Meyn, R. E. Clonogenic cell survival assay. *Methods Mol. Med.* **2005**, *110*, 21–28.